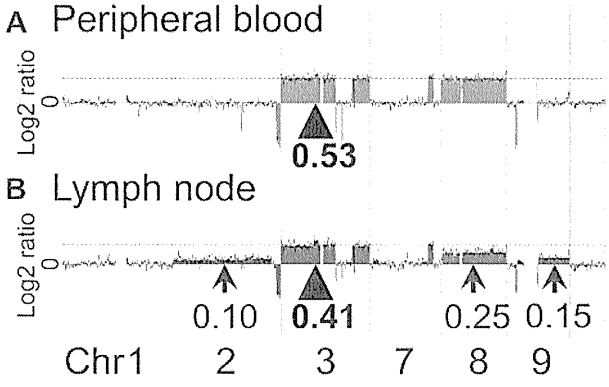

Figure 1. Representative profiles of the PB and LN samples of case 1. Array CGH results for case 1 are shown. (A) In the PB sample of case 1, regions of gain were detected. The log2 ratio of chromosome 3 was 0.53 (arrowhead). The log2 ratios of chromosomes 7 and 8 were the same as for chromosome 3 (dotted line). (B) In the LN sample of case 1, a log2 ratio imbalance was found. Log2 ratios among chromosomes 2, 3, 7, 8, and 9 differed. The log2 ratios of chromosome 3 and 7 were 0.41 (arrowhead and dotted line). Arrows show different log2 ratios: chromosome 2 = 0.10, chromosome 8 = 0.25, and chromosome 9 = 0.15.

57 years (range, 32-74 years). Detailed patient information is provided in supplemental Table 1 (available on the *Blood* Web site; see the Supplemental Materials link at the top of the online article).

Four cell lines, SP-49,[9] HANK1,[10] ATN-1,[11] and Jurkat,[12] were also analyzed. SP-49 is a mantle cell lymphoma cell line, HANK1 is a natural killer/T-cell lymphoma line, ATN-1 is an ATLL cell line, and Jurkat is a T-cell lymphoblast–like cell line.

Peripheral blood samples were obtained from the blood of 8 healthy male donors. PBMCs were isolated by Ficoll-Paque PLUS centrifugation (GE Healthcare).

DNA extraction

$CD4^+$ cells in PB samples were purified using a magnetic-activated cell-sorting protocol (Miltenyi Biotec). High–molecular-weight DNA was extracted from $CD4^+$ cells, frozen LNs, and from the SP-49, HANK1, ATN-1, and Jurkat cell lines using standard proteinase K treatment and phenol-chloroform extraction.[13] Normal DNA was obtained from PBMC samples of 8 healthy male donors.

Oligo-array CGH

Characterization of the genomic aberrations was performed using Agilent 44K Whole Human Genome CGH arrays (Agilent Technologies) containing 44 000 probes. Procedures for DNA digestion, labeling, hybridization, scanning, and data analyses were performed according to the manufacturer's protocol (Agilent Technologies).

CGH data analysis

CGH data were extracted from scanned images using Feature Extraction software (version 10.3; Agilent Technologies). Raw data were transferred to the Genomic Workbench v5.0 software (Agilent Technologies) for further analysis. We defined gains and losses over a continuous 15-probe dataset as a linear log2 ratio average of ≥ 0.05 or ≤ -0.05, respectively, and microdeletion for a range of 3-15 probes as a linear log2 ratio average of ≤ -0.4. A detailed explanation of the log2 ratio is available in the supplemental data. The array CGH data have been deposited in ArrayExpress under the accession number E-MEXP-3042.

Southern blot analysis of HTLV-1 integration and TCRγ rearrangement

Integration of the HTLV-1 provirus genome and TCRγ rearrangement were assayed as described previously.[5,14] In brief, DNA samples (5 μg) of LNs were digested with restriction enzymes (PstI) and electrophoresed through 0.7% agarose gels. The DNA was then transferred onto a Hybond N^+ membrane (Amersham Pharmacia Biotech) and hybridized to randomly primed ^{32}P-labeled DNA probes specific for the HTLV-1 and TCRγ genes. Blots were then washed at the appropriate stringency and visualized by autoradiography. The HTLV-1 probe comprised a 1.0-kb fragment of the pX region, which was PCR amplified using the primers 5′-ccacttcccagggtttggacag-3′ and 5′-tctgcctctttttcgttaaaaagtagagaaatggg-3′, and the TCRγ probe comprised a 0.6-kb fragment of Jγ2.1.[14]

Results

Oligo-array CGH analysis against paired samples obtained from the PB and LNs

In all of the 13 acute-type ATLL cases, genomic aberrations were detected by oligo-array CGH. Representative profiles of the paired samples obtained from the PB and LNs in cases 1 and 2 are shown in Figure 1A and B and Figure 2A and B, respectively.

In the PB sample of case 1, genomic aberration regions showed a constant log2 ratio. Regions of gain were detected on chromosomes 3, 7, and 8. The log2 ratios corresponding to these regions were 0.53, suggesting that there was no imbalance (Figure 1A arrowhead). On the other hand, imbalance of the log2 ratio among chromosomes was found for the LN sample of case 1. Genomic aberrations of the case 1 LN sample were similar to

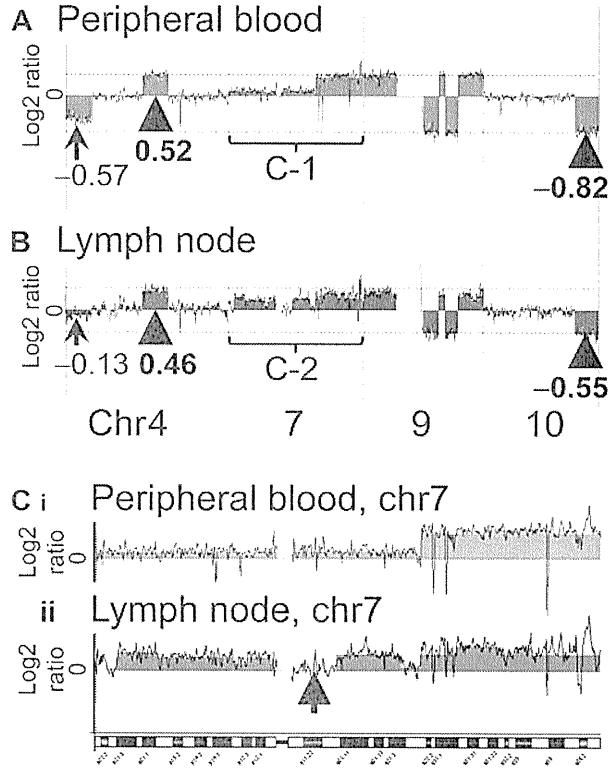

Figure 2. Representative profiles of the PB and LN samples of case 2. The results for case 2 were more complex than those for case 1. In both the PB and the LN samples of case 2, a log2 ratio imbalance was found. (A) In the PB sample, the arrowhead and dotted line indicate the majority of log2 ratios of gain and loss regions. Log2 ratios of the majority of loss regions were −0.82. The log2 ratio of chromosome 4 was −0.57. (B) In the LN sample, the arrowhead and dotted line indicate the majority of log2 ratios of gain and loss regions. Log2 ratios of the majority of loss regions were −0.55. The log2 ratio of chromosome 4 was −0.13. Chromosome 7 regions of PB and LN samples are magnified as Ci and Cii, respectively. (C) Chromosome 7 of the case 2 PB sample shows complex aberrations (i). This result also indicates a log2 ratio imbalance. Chromosome 7 of the case 2 LN sample shows more complex aberrations (ii). An arrow indicates a region (7q11.21-11q.23) without genomic aberration. Ci and Cii suggest that the genomic profiles of the PB and LN samples differ.

Table 1. Array CGH results of paired samples of acute-type ATLL

Case no.	Genome aberrations	Log2 imbalance		Genomic profiles of PB and LN	Common aberration regions between PB and LN	ATLL clones
		PB	LN			
1	+	−	+	different	+	Multiple subclones
2	+	+	+	different	+	Multiple subclones
3	+	−	−	same	+	Monoclone
4	+	+	+	different	+	Multiple subclones
5	+	+	−	different	+	Multiple subclones
6	+	−	−	same	+	Monoclone
7	+	+	+	different	+	Multiple subclones
8	+	−	+	different	+	Multiple subclones
9	+	−	+	different	+	Multiple subclones
10	+	−	+	different	+	Multiple subclones
11	+	−	−	same	+	Monoclone
12	+	−	−	same	+	Monoclone
13	+	+	+	different	+	Multiple subclones
Total	13 (100%)	5 (38.4%)	8 (61.5%)	9 (69.2%)	13 (100%)	9 (69.2%)

+ indicates present; and −, absent.

that of the PB sample. However, the log2 ratios among chromosomes 2, 3, 7, 8, and 9 differed as follows. Regions of gain were detected on chromosomes 2, 3, 7, 8, and 9, as shown by the log2 ratios: chromosome 2 = 0.10, chromosomes 3 and 7 = 0.41, chromosome 8 = 0.25, and chromosome 9 = 0.15 (Figure 1B arrowhead and arrows). The log2 ratio of chromosome 8 was lower than that of chromosomes 3 and 7. Gains of chromosomes 2 and 9 were detected in the LN sample, but not in the PB sample. These results indicated that a log2 ratio imbalance occurred in the LN sample.

Case 2 had a log2 ratio imbalance in both the PB and LN samples (Figure 2A). The genomic aberrations of the case 2 PB sample differed from those of the LN sample, as was also found with case 1. In the case 2 PB sample, regions of loss were detected on chromosomes 4, 9, and 10, as shown by the log2 ratios: chromosome 4 = −0.57 (Figure 2A arrow) and chromosomes 9 and 10 = −0.82 (Figure 2A arrowhead and dotted line). In the case 2 LN sample, regions of loss were also detected on chromosomes 4, 9, and 10, as shown by the log2 ratios: chromosome 4 = −0.13 (Figure 2B arrow) and, chromosomes 9 and 10 = −0.55 (Figure 2B arrowhead and dotted line). These data indicated that both samples had a log2 ratio imbalance. Complex genome aberrations were found for chromosome 7 in the paired samples of case 2. Consecutive gain regions were found in the whole of chromosome 7 of the PB sample (Figure 2Ci, and a region (7q11.21-11q.23) without genomic aberrations was found in chromosome 7 of the LN sample (Figure 2Cii arrow).

A log2 ratio imbalance among chromosomes was present in many other samples of acute-type ATLL, as summarized in Table 1.

Confirmation of log2 ratio imbalance among chromosomes

A log2 ratio imbalance among chromosomes was found in many ATLL clinical samples. We expected that a log2 ratio imbalance would indicate the presence of clones with different genomic aberrations. Therefore, we prepared 2 cell lines, SP-49 and HANK1, which possess different genomic aberrations. The genomic DNA of SP-49 was mixed with that of HANK1. We then conducted oligo-array CGH using the mixed-genomic DNA samples at various ratios.

Array CGH analysis of the SP-49 genome showed some genomic aberration regions, which were consistent with the G-band result that had been reported.[9] Log2 ratios of all 1-copy gain regions were 0.55, and log2 ratios of all 1-copy loss regions were −0.80. Imbalance of the log2 ratio among the chromosomes was not found. The same was true for HANK1, in which genomic aberration regions were consistent with the G-band result that had been reported and an imbalance of the log2 ratio among the chromosomes was not found.[10]

A representative array CGH result using a mixed-DNA sample at a ratio of 7:3 (SP-49:HANK1) is shown in Figure 3. The results showed an imbalance of the log2 ratio among chromosomes. It was possible to reproduce the log2 ratio imbalance. For example, the log2 ratios of chromosomes 2p14-pter, 2q14.3-qter, and 7p were 0.55, 0.15, and 0.46, respectively. These log2 ratios clearly differed. Furthermore, additional regions with different log2 ratios were found.

These results indicated that some of the clones present in the sample that had different genome profiles caused a log2 ratio imbalance in the array CGH result. The log2 ratio did not differ in chromosome 2p, which had a copy region identical to both SP-49 and HANK1.

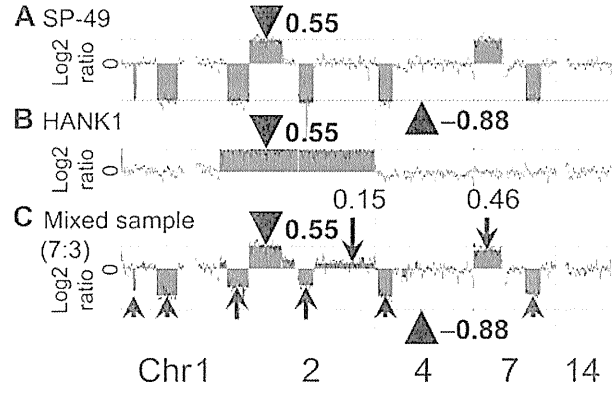

Figure 3. Confirmation of log2 ratio imbalance among chromosomes. The manner in which the log2 ratio imbalance occurred was confirmed. (A) SP-49 showed no imbalance. Log2 ratios of gain regions were 0.55 (arrowhead and dotted line). Log2 ratios of loss regions were −0.88 (arrowhead and dotted line). (B) HANK1 showed no imbalance. Log2 ratios of gain regions were 0.55 (arrowhead and dotted line). (C) Mixed-genomic DNA at a ratio of 7:3 reproduced the log2 ratio imbalance. The log2 ratio of chromosome 2p14-pter of the mixed DNA sample was 0.55 (arrowhead). Chromosome 2p had a copy region identical to both SP-49 and HANK1. Arrows indicate the log2 ratio imbalance.

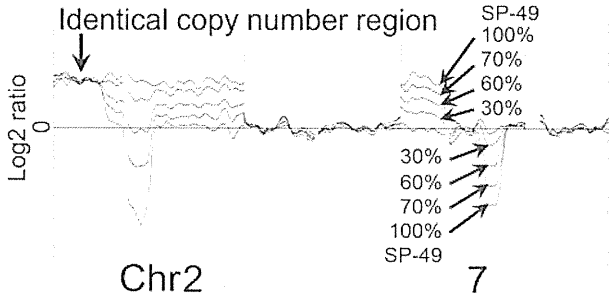

Figure 4. Log2 ratio reflects the ratio of tumor. The genome profiles of mixed-DNA samples comprising various ratios were superimposed. Gain was detected in chromosome 7 of all mixed samples, as shown by the log2 ratio: SP-49 = 0.55; 100%, 7:3 = 0.46; 70%, 6:4 = 0.32; 60%, 3:7 = 0.20; 30%. Loss was also detected in chromosome 7 of all mixed samples as shown by the log2 ratio: Sp-49 = −0.88; 100%, 7:3 = −0.62; 70%, 6:4 = −0.39; 60%, 3:7 = −0.14; 30%. Chromosome 2p had a copy region identical to both SP-49 and HANK1. The log2 ratios never changed in these regions.

Log2 ratios reflect the ratio of tumor

The genome profiles of mixed-DNA samples comprising various ratios were superimposed (Figure 4). The ratios of SP-49 to HANK1 were 7:3, 6:4, and 3:7. These results clearly revealed that the log2 ratio reflected the ratio of the tumor. When tumors included in a sample had identical genomic aberration regions, the log2 ratio never changed in these regions.

Southern blot analysis of HTLV-1 integration and TCRγ rearrangement

HTLV-1 integration

HTLV-1 integration was examined using Southern blot analysis, and the results showed HTLV-1 integration in all of the 11 cases examined. Eight of the 11 cases examined comprised a mono-integration band, whereas the others showed multi-integration bands. (Figure 5A)

TCRγ rearrangement

Southern blot analysis of TCR Jγ rearrangement was also conducted and evaluated as described previously by Moreau et al.[14] The results indicated that all samples were monoclonal (Figure 5B). Five of the 11 cases examined had a 6.8-kb rearrangement band, and 2 had a 2.9-kb rearrangement band. The others showed loss of germinal bands. In case 2, one allele of TCRγ was rearranged, because the germinal band of 8.0 kb was weaker than that of 4.9 kb. Case 7 lost all germinal bands, such as ATN-1, which is an ATLL cell line. This result indicated that both alleles of TCRγ were rearranged at Jγ2.3, because no deletion was found in case 7 by array CGH. Given that 3 or more TCR rearrangement bands were not found, no cases showed definite multi-clonality in tumor cells. These results indicated that the acute-type ATLL examined represented a monoclonal tumor comprising TCR rearrangements and with some possessing multiple integrations of HTLV-1.

Appearance of LN subclones before PB subclones

Array CGH analysis revealed that PB samples from 5 of 13 cases had homozygous loss regions that were not found in the corresponding LN samples of each case. In case 2, 1p12-1p13.1 of the PB sample was seen to represent homozygous loss, unlike the case with the LN sample (Figure 6). However, log2 ratios of same region in the LN sample seemed to be slightly lower than those of neighboring regions. This raised the possibility that a minor

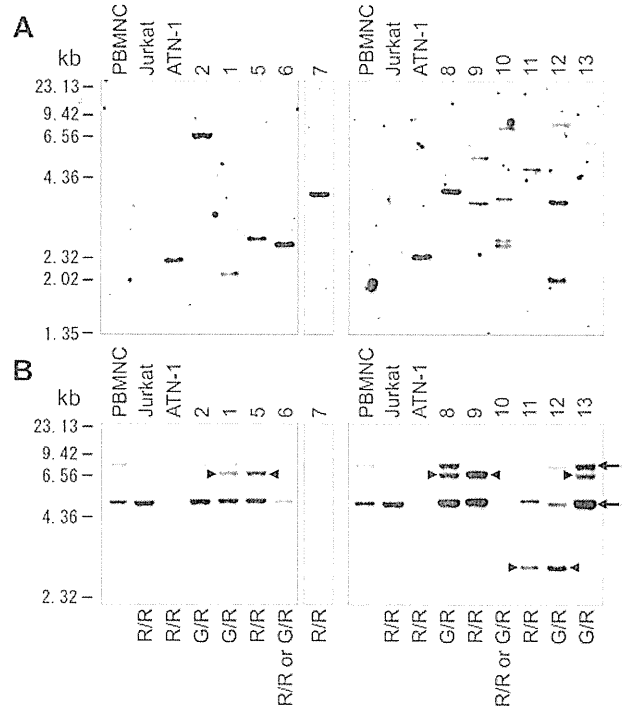

Figure 5. Southern blot analysis. (A) Southern blot analysis of HTLV-1 integration in 11 of 13 cases. (B) Southern blot analysis of TCRγ rearrangement. Arrows indicate the 8.00- and 4.9-kb germline bands. Arrowheads indicate the 6.8- and 2.9-kb rearrangement bands. G indicates a germinal allele; R, rearrangement allele; G/R, rearrangement of one allele; R/R, rearrangement of both alleles.

subclone was present. The PB samples from cases 1, 4, 8, and 10 also had homozygous loss regions that were not clearly found in the corresponding LN samples (Table 2).

No cases had a homozygous loss region in the LN samples when the PB samples had a heterozygous loss in the same regions. Array CGH and Southern blotting results indicated that multiple subclones had developed from one clone. Therefore, when 2 clones were found in a patient, the clone with homozygous loss must have developed from the clone with heterozygous loss. The homozygous loss analysis revealed that in about 40% of ATLL patients, subclones that had appeared in the PB were derived from LN subclones.

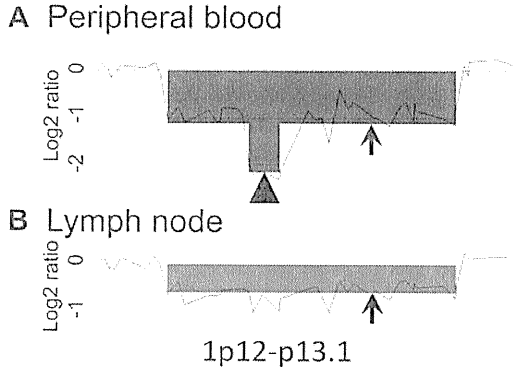

Figure 6. Homozygous loss region analysis. A representative homozygous loss region of case 2 is shown (1p12-p13.1). The total scale of the figure is approximately 2 Mb. The arrowhead indicates a homozygous loss region; arrows indicate heterozygous loss regions. Homozygous loss was found only in the PB sample. The log2 ratio of this region in the LN sample was slightly lower than that in the neighboring regions, suggesting the possibility that a minor subclone may exist in the LNs.

Table 2. PB samples of 5 of 13 cases only had homozygous loss regions that were not found in the LN samples

Case no.	Homozygous loss only in PB	Homozygous loss only in LN	Locus	Gene
1	+	–	3q22.3	*PCCB, STAG1*
2	+	–	1p12-p13.1	*IGSF3*
3	–	–		
4	+	–	6p22.3	*ATXN1*
5	–	–		
6	–	–		
7	–	–		
8	+	–	4q31.21	*INPP4B*
9	–	–		
10	+	–	9q31.2	*KLF4*
11	–	–		
12	–	–		
13	–	–		
Total	5	0		

+ indicates present; and –, absent.

Selected subclone of LNs in the PB

Tumor cells in the PB samples of some cases (eg, cases 1 and 9) appeared to have been selected from multiple subclones. In these cases, a log2 ratio imbalance was not found in the PB sample but was found in the LN sample. This indicated that PB samples were monoclonal and that the LN samples contained multiple subclones. Both samples from each case had common aberrations, and the LN samples had aberrations that were not found in the PB samples. These results may indicate that the LNs contain multiple subclones with different genomic aberrations, and that one of these subclones then appears in the PB (Figure 7).

Discussion

The imbalance and differing genomic profiles of PB and LN samples indicate that acute-type ATLL comprises multiple subclones

In this study, we revealed the presence of a log2 ratio imbalance among chromosomes of LN samples in many patients with acute-type ATLL. Most of the genomic profiles were found to differ from those of the PB samples. Although monoclonal proliferation of acute-type ATLL is referred to in the World Health Organization classification,[15] these data clearly show that acute-type ATLL contains multiple subclones that originate as a result of clonal evolution in ATLL patients.

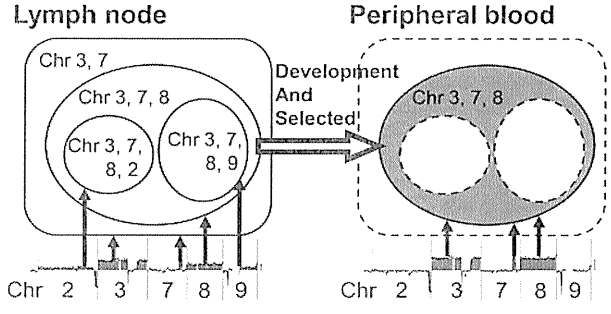

Figure 7. Selected subclone from the LN in the PB. Shown is a schematic representation of a selected subclone from the LN sample in the PB of case 1. In the LN sample of case 1, at least 4 subclones exist: a subclone with chromosome 3 and 7 aberrations; a subclone with additional chromosome 8 aberrations; a subclone with chromosome 3, 7, 8, and 2 aberrations; and a subclone with chromosome 3, 7, 8, and 9 aberrations. Among these subclones, a subclone with chromosome 3, 7, and 8 aberrations appeared in the PB sample.

Shinawi et al[16] reported a case of pediatric AML in which 2 clones with different chromosome aberrations showed a log2 ratio imbalance as detected by array CGH. We were able to reproduce a log2 ratio imbalance among chromosomes by mixing different ratios of DNA prepared from 2 different cell lines. The log2 ratio reflected the ratio of tumor clones. Based on these data, we analyzed the acute-type ATLL data and identified that a log2 ratio imbalance indicated the presence of multiple subclones in a sample. Minority clones with low log2 ratios could be found in this experiment by taking advantage of the high sensitivity associated with the use of array CGH. As a result, the presence of multiple subclones was unambiguously determined.

Cases showing different genomic profiles between PB and LN samples reached as high as 69%. We reported previously that paired samples obtained from different sites had different chromosomal aberrations in some cases.[17] We also reported that sequential samples at chronic and crisis or acute onset and relapse in each case showed different chromosome aberrations or integrations as determined by chromosomal CGH or Southern blot analysis.[17] Similar clonal change has been reported previously in some cases of B-cell lymphoma.[18] Although analysis of sequential samples is important when examining the stability of multiple subclones, it is difficult to acquire sequential samples from acute-type ATLL patients because these patients require immediate chemotherapy. However, chronic-type ATLL can be treated with "watchful waiting," so the clonal stability of ATLL may be explored in these patients.

Our data indicate that acute-type ATLL comprises multiple subclones with differing genomic aberrations. Several morphologic variants of ATLL have been described,[15] and the presence of a mixture of cells of different sizes has been reported. However, the histological type does not correspond to the clinical subtype.[19] Therefore, it is reasonable to postulate that the histological type does not always reflect the clinical features because the tumor subclones may differ at various sites.

HTLV-1 integration and TCRγ rearrangement determined by Southern blotting

We focused on the cell origin of the multiple subclones in each patient. Southern blot analysis revealed a monoclonal band of HTLV-1 integration or monoclonal rearrangement of TCRγ in all samples examined. These data indicated that the ATLL clones in each case had a common tumor cell origin. ATLL research and treatment utilize the Shimoyama classification. Acute-type ATLL represents one subtype in the classification, and is considered to be a monoclonal tumor. Our data are also consistent with this classification. However, it is possible that multiple subclones in the LNs possess a diversity that may account for the variable clinical manifestations and drug resistance that can occur during the treatment of ATLL.

Selection of leukemic clone and diversity in LNs

Array CGH suggested that the subclones in the PB and LNs differed even though they are derived from an identical monoclonal tumor cell, as determined by in Southern blot analysis. Given that the clones are derived from one clone, theoretically the clone with heterozygous loss is never derived from a cell with homozygous loss. Homozygous loss regions were only present in the PB samples examined at a frequency of 38% (5 of 13 cases examined). None of the 5 samples showed homozygous loss

regions found in the LN samples, indicating that in these cases, subclones present in the LNs were not derived from those in the PB. These results suggested that the selected subclones appeared in the PB after subclones developed in the LNs. However, it remains to be determined how these clones in the PB become stable during the course of disease. It is also important to determine whether the tumor cells in the PB can proliferate at the level of tumor cells in the LNs.

In conclusion, the results of the present study showed that there are multiple subclones in acute-type ATLL, all of which possess a common TCR rearrangement and the genomic profiles of which often differ between the PB and LNs. Cases were identified in which a selected subclone from multiple subclones in the LN samples was also identified in the PB samples. ATLL was clinically classified into 4 subtypes by Shimoyama. However, the specific genes that characterize acute-type ATLL have not been identified. Our results reveal that acute-type ATLL is a genetically heterogeneous neoplasm and that clonal evolution of ATLL takes place in the LNs.

Acknowledgments

We thank Dr Koichi Ohshima for diagnoses; Dr Shinobu Tsuzuki, Dr Kennosuke Karube, and Dr Keiichiro Honma for discussions and encouragement throughout this study; and Kyoko Hirano for outstanding technical assistance.

This work was supported in part by grants-in-aid from the Ministry of Health, Labor and Welfare of Japan; from the Ministry of Education, Culture, Sports, Science and Technology of Japan; and from the Japan Society for the Promotion of Science.

Authorship

Contribution: A. Umino performed the experiments, analyzed data, and wrote the paper; M.N. analyzed data and performed experiments; A. Utsunomiya provided advice, discussed clinical data, and treated patients; K.T. provided advice, discussed clinical data, treated patients, and wrote the paper; N.T. analyzed and discussed clinical data; N.K. discussed clinical data; and M.S. supervised the research, discussed clinical data, analyzed data, and wrote the paper.

Conflict-of-interest disclosure: The authors declare no competing financial interests.

Correspondence: Masao Seto, MD, PhD, Division of Molecular Medicine, Aichi Cancer Center Research Institute, 1-1 Kanokoden, Chikusa-ku, Nagoya, Aichi 464-8681, Japan; e-mail: mseto@aichi-cc.jp.

References

1. Shimoyama M. Diagnostic criteria and classification of clinical subtypes of adult T-cell leukaemia-lymphoma. A report from the Lymphoma Study Group (1984-87). *Br J Haematol.* 1991;79(3):428-437.
2. Raimondi SC, Behm FG, Roberson PK, et al. Cytogenetics of childhood T-cell leukemia. *Blood.* 1988;72(5):1560-1566.
3. Shimoyama M, Abe T, Miyamoto K, et al. Chromosome aberrations and clinical features of adult T cell leukemia-lymphoma not associated with human T cell leukemia virus type I. *Blood.* 1987; 69(4):984-989.
4. Maciejewski JP, Tiu RV, O'Keefe C. Application of array-based whole genome scanning technologies as a cytogenetic tool in haematological malignancies. *Br J Haematol.* 2009;146(5):479-488.
5. Oshiro A, Tagawa H, Ohshima K, et al. Identification of subtype-specific genomic alterations in aggressive adult T-cell leukemia/lymphoma. *Blood.* 2006;107(11):4500-4507.
6. Tsukasaki K, Tsushima H, Yamamura M, et al. Integration patterns of HTLV-I provirus in relation to the clinical course of ATL: frequent clonal change at crisis from indolent disease. *Blood.* 1997;89(3):948-956.
7. Etoh K, Tamiya S, Yamaguchi K, et al. Persistent clonal proliferation of human T-lymphotropic virus type I-infected cells in vivo. *Cancer Res.* 1997; 57(21):4862-4867.
8. Okamoto T, Ohno Y, Tsugane S, et al. Multi-step carcinogenesis model for adult T-cell leukemia. *Jpn J Cancer Res.* 1989;80(3):191-195.
9. Daibata M, Takasaki M, Hirose S, et al. Establishment of a new human B cell line carrying t(11;14) chromosome abnormality. *Jpn J Cancer Res.* 1987;78(11):1182-1185.
10. Kagami Y, Nakamura S, Suzuki R, et al. Establishment of an IL-2-dependent cell line derived from 'nasal-type' NK/T-cell lymphoma of CD2+, sCD3-, CD3epsilon+, CD56+ phenotype and associated with the Epstein-Barr virus. *Br J Haematol.* 1998;103(3):669-677.
11. Naoe T, Akao Y, Yamada K, et al. Cytogenetic characterization of a T-cell line, ATN-1, derived from adult T-cell leukemia cells. *Cancer Genet Cytogenet.* 1988;34(1):77-88.
12. Gillis S, Watson J. Biochemical and biological characterization of lymphocyte regulatory molecules. V. Identification of an interleukin 2-producing human leukemia T cell line. *J Exp Med.* 1980;152(6):1709-1719.
13. Seto M, Yamamoto K, Iida S, et al. Gene rearrangement and overexpression of PRAD1 in lymphoid malignancy with t(11;14)(q13;q32) translocation. *Oncogene.* 1992;7(7):1401-1406.
14. Moreau EJ, Langerak AW, van Gastel-Mol EJ, et al. Easy detection of all T cell receptor gamma (TCRG) gene rearrangements by Southern blot analysis: recommendations for optimal results. *Leukemia.* 1999;13(10):1620-1626.
15. Ohshima K, Jaffe ES, Kikuchi M. Adult T-cell leukaemia/lymphoma. In: The National Agency for Research on Cancer, Swerdlow S, Campo E, Lee Harris N, et al, eds. *WHO Classification of Tumours of Haematopoietic and Lymphoid Tissues.* Lyon: World Health Organization; 2008: 281-284.
16. Shinawi M, Erez A, Shardy DL, et al. Syndromic thrombocytopenia and predisposition to acute myelogenous leukemia caused by constitutional microdeletions on chromosome 21q. *Blood.* 2008;112(4):1042-1047.
17. Tsukasaki K, Krebs J, Nagai K, et al. Comparative genomic hybridization analysis in adult T-cell leukemia/lymphoma: correlation with clinical course. *Blood.* 2001;97(12):3875-3881.
18. Siegelman MH, Cleary ML, Warnke R, Sklar J. Frequent biclonality and Ig gene alterations among B cell lymphomas that show multiple histologic forms. *J Exp Med.* 1985;161(4):850-863.
19. Takeshita M, Akamatsu M, Ohshima K, et al. CD30 (Ki-1) expression in adult T-cell leukaemia/lymphoma is associated with distinctive immunohistological and clinical characteristics. *Histopathology.* 1995;26(6):539-546.

Overexpression of enhancer of zeste homolog 2 with trimethylation of lysine 27 on histone H3 in adult T-cell leukemia/lymphoma as a target for epigenetic therapy

Daisuke Sasaki,[1] Yoshitaka Imaizumi,[2] Hiroo Hasegawa,[1] Akemi Osaka,[1] Kunihiro Tsukasaki,[2] Young Lim Choi,[3] Hiroyuki Mano,[3] Victor E. Marquez,[4] Tomayoshi Hayashi,[5] Katsunori Yanagihara,[1] Yuji Moriwaki,[2] Yasushi Miyazaki,[2] Shimeru Kamihira,[1] and Yasuaki Yamada[1]

[1]Department of Laboratory Medicine, Nagasaki University Graduate School of Biomedical Sciences, Nagasaki, Japan; [2]Department of Hematology and Molecular Medicine, Atomic Bomb Disease Institute, Nagasaki University Graduate School of Biomedical Sciences, Nagasaki, Japan; [3]Division of Functional Genomics, Jichi Medical University, Tochigi, Japan; [4]Chemical Biology Laboratory, National Cancer Institute, Frederick, MD, USA; and [5]Department of Pathology, Nagasaki University Hospital, Nagasaki, Japan

ABSTRACT

Background
Enhancer of zeste homolog 2 is a component of the Polycomb repressive complex 2 that mediates chromatin-based gene silencing through trimethylation of lysine 27 on histone H3. This complex plays vital roles in the regulation of development-specific gene expression.

Design and Methods
In this study, a comparative microarray analysis of gene expression in primary adult T-cell leukemia/lymphoma samples was performed, and the results were evaluated for their oncogenic and clinical significance.

Results
Significantly higher levels of Enhancr of zeste homolog 2 and RING1 and YY1 binding protein transcripts with enhanced levels of trimethylation of lysine 27 on histone H3 were found in adult T-cell leukemia/lymphoma cells compared with those in normal $CD4^+$ T cells. Furthermore, there was an inverse correlation between the expression level of Enhancer of zeste homolog 2 and that of miR-101 or miR-128a, suggesting that the altered expression of the latter miRNAs accounts for the overexpression of the former. Patients with high Enhancer of zeste homolog 2 or RING1 and YY1 binding protein transcripts had a significantly worse prognosis than those without it, indicating a possible role of these genes in the oncogenesis and progression of this disease. Indeed, adult T-cell leukemia/lymphoma cells were sensitive to a histone methylation inhibitor, 3-deazaneplanocin A. Furthermore, 3-deazaneplanocin A and histone deacetylase inhibitor panobinostat showed a synergistic effect in killing the cells

Conclusions
These findings reveal that adult T-cell leukemia/lymphoma cells have deregulated Polycomb repressive complex 2 with over-expressed Enhancer of zeste homolog 2, and that there is the possibility of a new therapeutic strategy targeting histone methylation in this disease.

Key words: adult T-cell leukemia/lymphoma, human T-cell leukemia virus type-1, Enhancer of zeste homolog 2, H3K27me3.

Citation: Sasaki D, Imaizumi Y, Hasegawa H, Osaka A, Tsukasaki K, Choi YL, Mano H, Marquez VE, Hayashi T, Yanagihara K, Moriwaki Y, Miyazaki Y, Kamihira S, and Yamada Y. Overexpression of enhancer of zeste homolog 2 with trimethylation of lysine 27 on histone H3 in adult T-cell leukemia/lymphoma as a target for epigenetic therapy Haematologica 2011;96(4):712-719. doi:10.3324/haematol.2010.028605

Funding: supported in part by a Grant-in-Aid for Scientific Research from the Ministry of Health, Labour, and Welfare of Japan (N. 04010119). For VEM, this research was supported in part by the Intramural Research Program of the NIH, Center for Cancer Research, NCI-Frederick.

Acknowledgments: the authors thank Sayaka Mori and Yuko Doi for excellent technical assistance.

Manuscript received June 16, 2010. Revised version arrived on December 16, 2010. Manuscript accepted on December 31, 2010.

Correspondence:
Yasuaki Yamada, Department of Laboratory Medicine, 1-7-1 Sakamoto, Nagasaki 852-8501, Japan. Phone: international +81.958197408.
Fax: international +81.958197422.
E-mail: y-yamada@nagasaki-u.ac.jp

The online version of this article has a Supplementary Appendix.

Introduction

The Polycomb group (PcG) proteins play critical roles in the regulation of development by repressing specific sets of developmental genes through chromatin modification.[1] They form two distinct multimeric complexes, Polycomb repressive complex 1 (PRC1) and PRC2, which bind to polycomb responsive elements (PRE), repress genes required for cell differentiation, and maintain pluripotency and self-renewal of embryonic stem cells and hematopoietic stem cells.[2,3] PRC2 consists of Enhancer of zeste homolog 2 (EZH2), which has histone methyltransferase activity, suppressor of zeste 12 (SUZ12), and embryonic ectoderm development (EED), which is required to maintain the integrity of PRC2.[1,4] Sequence-specific DNA binding protein YY1, which recognizes PRE, interacts with EED and recruits PRC2 to a specific chromatin domain to be repressed.[5] EED interacts with histone deacetylase (HDAC) proteins, HDAC1 and HDAC2, and the histone binding proteins RBBP4 (RbAp48) and RBBP7 (RbAp46).[6] PRC2 thus also participates in histone deacetylation. EZH2, as a part of the PRC2 complex, not only methylates histone but also serves as a recruitment platform for DNA methyltransferases that methylate the promoter regions of target genes, which is another mechanism of gene repression.[7] The more diverse complex PRC1 consists of HPC family proteins that mediate chromatin association, HPH family proteins, RING, BMI1, and others.[1] PRC2 initiates trimethylation of lysine 27 on histone H3 (H3K27me3) and, to a lesser extent, lysine 9 of histone H3.[8] PRC1 recognizes H3K27me3 through the chromodomain of the HPC and maintains the trimethylation. There are a number of reports indicating that such epigenetically mediated transcriptional silencing is associated with cancer development.[1,9] Among these, oncogenic roles of over-expressed EZH2 have been studied in a variety of tumors.[10]

Adult T-cell leukemia/lymphoma (ATL) is a neoplasm of mature CD4+ T-cell origin, etiologically associated with human T-cell leukemia virus type-1 (HTLV-1).[11,12] Its clinical behavior differs among patients and is subclassified into four subtypes: smoldering type and chronic type as indolent subtypes, and acute type and lymphoma type as aggressive subtypes.[13] Inactivation of tumor suppressor genes is one of the key events in development and progression, and there is a strong accumulation of *p14ARF/p15INK4B/p16INK4A* gene deletion/methylation or *p53* gene mutations in aggressive subtypes (>60%).[14-20] In the present study, for further investigation of the oncogenesis of ATL, we performed a comparative microarray analysis of gene expression in primary ATL samples. ATL cells expressed significantly higher levels of *EZH2* and *RYBP* (RING1 and YY1 binding protein) transcripts than CD4+ T cells from healthy volunteers. Moreover, acute-type ATL cells showed significantly higher levels of these transcripts than chronic-type ATL cells, suggesting that deregulation of PcG proteins plays a crucial role not only in the development but also in the progression of ATL. In addition, ATL samples were strongly positive for H3K27me3, and were sensitive to 3-deazaneplanocin A (DZNep), a histone methylation inhibitor.[21-23] It has recently been shown that HDAC inhibitor panobinostat (PS, also known as LBH589) depletes the levels of EZH2, SUZ12, and EED and induces apoptotic death in leukemia cells.[24] Deregulation of PcG protein genes with over-expressed EZH2 in ATL cells suggests that ATL is one of the appropriate target diseases for such epigenetic therapy.

Design and Methods

Sample preparation

This study was approved by the ethics committees of Nagasaki University, and all clinical samples were obtained after written informed consent was provided. The diagnosis of ATL was confirmed by the monoclonal integration of HTLV-1 proviral DNA in the genomic DNA of leukemia cells. Peripheral blood mononuclear cells (PBMCs) were obtained from ATL patients (acute type 22 cases, chronic type 19 cases) and healthy adult volunteers by density gradient centrifugation using Lympho-prep (AXIS SHIELD, Oslo, Norway). For enrichment of ATL cells, CD4+ cells were purified from the PBMCs by the magnetic bead method (CD4 MicroBeads, Miltenyi Biotec, Auburn, CA, USA) as described elsewhere.[25] Besides these samples for microarray analysis, we prepared another set of samples for quantitative real-time RT-PCR (qRT-PCR) and Western blotting (25 ATL patients, 13 HTLV-1 carriers, and 12 healthy adults) to confirm the results of microarray analysis. We also used formalin-fixed, paraffin-embedded lymph nodes from 7 patients with lymphoma-type ATL and 5 patients with follicular lymphoma for immunohistochemical analysis.

ATL cell lines used in this study, SO4, ST1, KK1, KOB, and LM-Y1, were established from respective patients in our laboratory and have been confirmed to be of primary ATL cell origin.[26] Cells were maintained in RPMI1640 medium supplemented with 10% FBS and 100 Japan reference units of recombinant interleukin-2 (rIL-2) (kindly provided by Takeda Pharmaceutical Company, Ltd., Osaka, Japan). We also used HTLV-1-infected T-cell lines MT2 and HuT102 and acute T-lymphoblastic leukemia cell lines Jurkat and MOLT4, which were maintained without rIL-2.

DNA microarray analysis

RNA was prepared from purified CD4+ T cells, and subjected to hybridization to HGU133A & B microarray containing 44,760 probe sets for human genes (Affymetrix, Santa Clara, CA, USA) as described previously.[25,27] The mean expression intensity of the internal positive control probe sets (*http://www.affymetrix.com/support/technical/mask_files.affx*) was set to 500 units in each hybridization, and the fluorescence intensity of each test gene was normalized accordingly. All HGU133A & B microarray data are available from the Gene Expression Omnibus website (*http://www.ncbi.nlm.nih.gov/geo*) under the accession number GSE1466.

Quantitative real-time RT-PCR

For confirmation of the results of microarray analysis, we performed quantitative real-time RT-PCR (qRT-PCR) for PcG protein genes. Total RNA was prepared using Isogen (Wako, Osaka, Japan). After removal of contaminated DNA with DNase (Message Clean kit; GenHunter, Nashville, TN, USA), cDNA was constructed from 1 μg of total RNA using the SuperScript III RT-PCR System (Invitrogen, Carlsbad, CA, USA) according to the manufacturer's instructions. Primers and TaqMan probes labeled with TAMRA dye at the 3' end and FAM at the 5' end are listed in *Online Supplementary Table S1*. The mRNA levels for PcG family proteins and porphobilinogen deaminase (PBGD) were measured from a cDNA template using a LightCycler480 PCR System (Roche Diagnostics, Mannheim, Germany). Briefly, reactions were performed in a 20 μL volume with 5 μL (25 ng) of cDNA, 0.5 μM PCR primers, 0.1 μM TaqMan probes, and 10 μL of LightCycler

480 probes Master Mix (Roche Diagnostics). The PCR program consisted of 95°C for 5 min followed by 50 cycles of 95°C for 10 sec and 60°C for 30 sec. After 50 cycles, the absolute amounts of PcG protein mRNA and *PBGD* mRNA were interpolated from the standard curves generated by the dilution method using plasmids derived from a clone transfected with pTAC-1 Vector (BioDynamics Laboratory Inc., Tokyo, Japan) containing amplicons from the PcG family protein and PBGD genes, respectively. To normalize these results for variability in concentration and integrity of RNA and cDNA, the *PBGD* gene was used as an internal control in each sample.

For the quantitative PCR for microRNAs (miRNAs), miR-101, miR-26a, and miR-128a, 10 ng of total RNA (containing miRNA) was used. RT reaction and real-time quantification were performed using TaqMan MicroRNA RT kit and TaqMan MicroRNA assays (hsa-miR-26a, assay ID 000405; hsa-miR-101, assay ID 002253; hsa-miR-128a, assay ID 002216; RNU6B, assay ID 001093) (Applied Biosystems, Foster City, CA, USA) in accordance with the manufacturer's instructions. Each PCR reaction mixture contained 10 μL of LightCycler 480 probes Master Mix, 4 μL of nuclease-free water, 1 μL of 20X specific PCR primer, and 5 μL of RT product. The thermal cycler was programmed as follows: 95°C for 5 min, 40 cycles of 95°C for 15 sec, and 60°C for 60 sec. Using the comparative CT method, we used an endogenous control (RNU6B) to normalize the expression levels of target micro-RNA by correcting differences in the amount of RNA loaded into qPCR reactions.

Western blot analysis and antibodies

Western blot analysis was performed as described previously.[28] The analysis was performed using antibodies to EZH2 and Histone H3 (Cell Signaling Technology, Danvers, MA, USA), phospho EZH2 (Ser21) (Bethyl Laboratories, Montgomery, TX, USA), H3K27me3, dimethylated H3K27 (H3K27me2), monomethylated H3K27 (H3K27me1) (Millipore, Temecula, CA, USA), and β-actin (Sigma, St. Louis, MO, USA).

Immunohistochemistry

Immunohistochemical staining for EZH2 and H3K27me3 was performed on formalin-fixed, paraffin-embedded lymph node samples from lymphoma-type ATL patients and follicular lymphoma patients as a control. The deparaffinized slides were pretreated with DAKO Target Retrieval Solution, pH 9 (DAKO Japan, Tokyo, Japan), and heated in a water bath at 95°C for 40 min. For all stains, the endogenous peroxidase was quenched using 3% H_2O_2 for 15 min. Sections were then placed in 0.5% non-fat dry milk for 30 min at room temperature. The primary antibodies used were anti-EZH2 antibody (BD Biosciences, San Jose, CA, USA) and anti-H3K27me3 antibody (Cell Signaling Technology, Boston, MA, USA), and were applied at 1:50 dilution and 1:100 dilution, respectively. They were allowed to react for 1 h at room temperature, and then the DAKO EnVision™ + Dual Link System-HRP (DAKO Japan, Tokyo, Japan) was applied using diaminobenzidine as the chromogen, following the manufacturer's protocol.

Sensitivity of adult T-cell leukemia/lymphoma cell lines to DZNep and PS (LBH589)

DZNep was synthesized by one of the authors (VEM). Cells were treated with different concentrations of DZNep for 72 h and the cell proliferation status was evaluated by an MTS assay using a Cell Titer 96® AQueos Cell Proliferation Assay kit (Promega, Madison, WI, USA) in accordance with the manufacturer's instructions. To analyze the synergistic effect of combined treatment with DZNep and PS (LBH589) (kindly provided by Novartis Pharma AG, Basel, Switzerland), cells were treated with DZNep (0.3-5.0 μM) and PS (LBH589) (3-50 nM) for 48 h. After the cell proliferation status was evaluated by an MTS assay, the combination index (CI) for each drug combination was obtained by determining the median dose effect of Chou and Talalay using the CI equation within the commercially available software Calcusyn (Biosoft).[29] CI<1, CI=1, and CI>1 indicate synergism, additive effect, and antagonism, respectively. Cell viability represents the value relative to that of the control culture without these agents.

Results

Microarray analysis shows increased EZH2 and/or RYBP transcripts in adult T-cell leukemia/lymphoma cells

In a comparative microarray analysis of primary ATL samples, we focused on investigating PcG protein genes, *EZH2*, *RYBP*, *BMI-1*, and *CBX7*, in the present study because ATL cells show many aberrantly hypermethylated DNA sequences.[30] ATL cells expressed significantly higher levels of *EZH2* and *RYBP* transcripts than $CD4^+$ T cells from healthy adults (Figure 1A and B). In addition, there was a difference between ATL subtypes in these expressions, and cells from the acute type showed significantly higher levels of these transcripts than the cells from the chronic type. When patients were separated into two groups consisting of those with high expression and those with low expression, the group with high *EZH2* or high *RYBP* transcript showed significantly shorter survival than the respective low-expression groups (Figure 1E and F), indicating that high *EZH2* and/or *RYBP* expression is associated with aggressive clinical behavior. Convincingly, there was a trend toward accumulation of acute-type ATL in the high *EZH2* or the high *RYBP* expression group: 14 cases of acute type and 6 cases of chronic type in the high *EZH2* group, 7 cases of acute type and 13 cases of chronic type in the low *EZH2* group, 14 cases of acute type and 6 cases of chronic type in the high RYBP group, and 7 cases of acute type and 13 cases of chronic type in the low RYBP group. BMI1 is known to down-regulate the expression of *p14ARF/p16INK4A* and lead to neoplastic transformation.[31] Chromobox 7 (CBX7), a component of the PRC1, is also known to repress the transcription of *p14ARF/p16INK4A*.[32] Since inactivation of *p14ARF/p15INK4B/p16INK4A* genes is one of the key events in ATL progression, expression of *BMI-1* and/or *CBX7* transcript was expected to be elevated in acute-type ATL cells. There was, however, no difference in these expressions between ATL subtypes or even between ATL cells and normal $CD4^+$ T cells (Figure 1C and D). There was no difference in survival for different *BMI-1* or *CBX7* expression levels (Figure 1G and H).

Confirmation of increased EZH2 and/or RYBP transcripts by quantitative real-time RT-PCR

For confirmation of the results of microarray analysis, we quantified the transcripts of the PcG protein genes including *EZH2* and *RYBP* by qRT-PCR using another set of samples from ATL patients, healthy adults, HTLV-1 carriers, and hematologic cell lines including ATL cell lines. In accordance with the results of microarray analysis, *EZH2* and *RYBP* transcripts were increased in primary ATL cells compared with those in the cells from healthy adults and HTLV-1 carriers, with statistically significantly higher val-

ues in *EZH2* in terms of both absolute copy number per 25 ng of total RNA and normalized expression level (*Online Supplementary Figure S1A, a, B, b*). *RBBP4* was significantly higher in primary ATL cells than in the cells from healthy adults and HTLV-1 carriers in terms of normalized expression level (*Online Supplementary Figure S1 C, c*). In contrast, there was no difference in *BMI1*, *YY1*, and *EED* expressions among these groups, although some patients showed very high *BMI1* expression (*Online Supplementary Figure S1D, d, E, e, F, f*). Similarly to primary ATL cells, some ATL cell lines showed high *EZH2* expression in terms of absolute copy number per 25 ng of total RNA (*Online Supplementary Figure S1A*).

EZH2 protein expression with trimethylation of H3K27 is characteristic in adult T-cell leukemia/lymphoma cells

We then examined EZH2 and RYBP at the protein level by Western blotting. A 98-kDa band for EZH2 protein and a 32-kDa band for RYBP protein were detected in all primary ATL samples irrespective of subtype, but they were hardly detected in cells from healthy adults and HTLV-1 carriers (Figure 2A, *Online Supplementary Figure S2*, and *data not shown*). ATL cell lines and acute T-lymphoblastic leukemia cell lines also showed intense EZH2 bands. The serine-threonine kinase Akt phosphorylates EZH2 at serine 21 and suppresses its methyltransferase activity by impeding EZH2 binding to histone H3, which results in a decrease in lysine 27 trimethylation.[33] EZH2 of ATL cells was not phosphorylated and was in its active form (Figure 2A). In fact, most primary ATL samples showed the band for H3K27me3, while the cells from healthy adults lacked the band (Figure 2B). As it is known that EZH2 plays a crucial role in trimethylation but not in dimethylation or monomethylation, the bands for H3K27me2 and H3K27me1 were detected in all samples examined, but the band for H3K27me3 was limited in primary ATL cells and ATL cell lines LMY1 and KOB that showed an intense EZH2 band with a faint phosphorylated EZH2 band (Figure 2A and B). In contrast, EZH2 was strongly phosphorylated in ATL cell lines ST1, SO4, KK1, and acute T-lymphoblastic leukemia cell lines Jurkat and MOLT4, and these cell lines hardly showed the band for H3K27me3. Collectively, these results indicate that ATL cells express

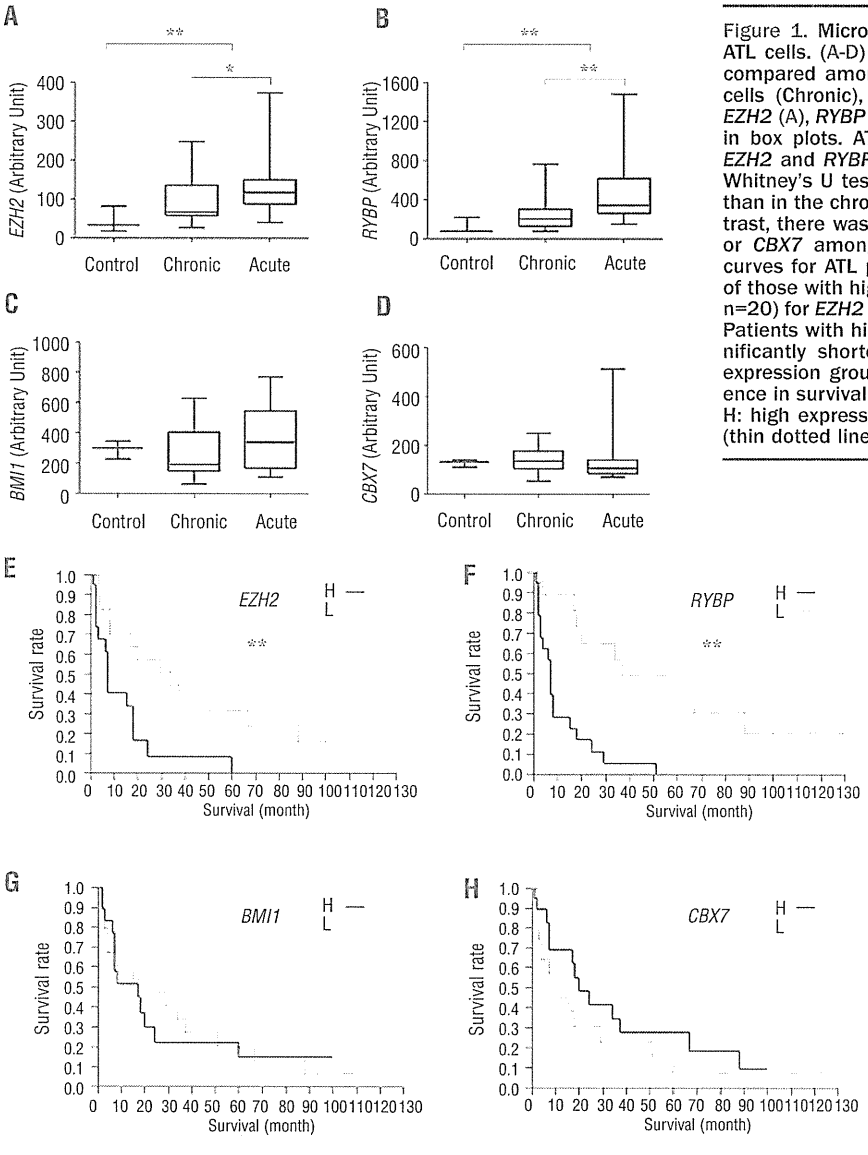

Figure 1. Microarray analysis of gene expression in primary ATL cells. (A-D) Expression levels of PcG protein genes were compared among normal CD4+ T cells (Control), chronic ATL cells (Chronic), and acute ATL cells (Acute), and results of *EZH2* (A), *RYBP* (B), *BMI1* (C), and *CBX7* (D) are demonstrated in box plots. ATL cells showed significantly higher levels of *EZH2* and *RYBP* transcripts than normal CD4+ T cells (Mann-Whitney's U test), with a higher expression in the acute type than in the chronic type (Mann-Whitney's U test) (A, B). In contrast, there was no statistical difference in the level for *BMI1* or *CBX7* among these groups (C, D). (E-H) Overall survival curves for ATL patients separated into two groups consisting of those with high expression (H, n=20) and low expression (L, n=20) for *EZH2* (E), *RYBP* (F), *BMI1* (G), or *CBX7* (H) are shown. Patients with high *EZH2* or high *RYBP* expression showed significantly shorter survival than those in corresponding low expression groups (log rank test) (E, F). There was no difference in survival for different *BMI1* or *CBX7* expressions (G, H). H: high expression group (bold line), L: low expression group (thin dotted line). $*P<0.05$, $**P<0.01$

functionally active EZH2, and as a result, their H3K27 are trimethylated, and that ATL cell lines LMY1 and KOB preserve this characteristic of primary ATL cells.

Immunohistochemical confirmation of the expression of EZH2 and H3K27me3 in lymph nodes

We next used lymph nodes from lymphoma-type ATL patients for immunohistochemical evaluation of EZH2 expression and H3K27me3. In agreement with the results of Western blotting, all ATL lymph nodes from 7 patients were strongly positive for both EZH2 and H3K27me3 without exception in their nuclear staining (*Online Supplementary Figure S3* and *data not shown*), suggesting that overexpression of EZH2 with H3K27me3 is a common feature of ATL cells irrespective of ATL subtypes. In contrast, in lymph nodes from 5 follicular lymphoma patients, only a few cells were positive for EZH2 with some variation among patients and most cells were negative for H3K27me3 (*Online Supplementary Figure S3* and *data not shown*).

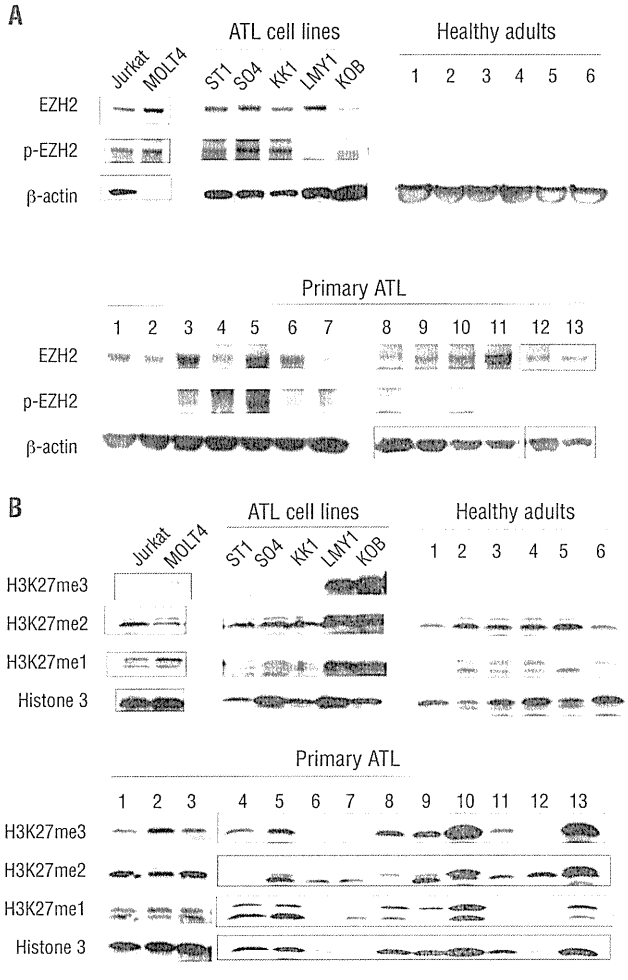

Figure 2. EZH2 protein expression and histone methylation. (A) Western blot analysis for EZH2 protein was performed on primary ATL cells, cells from healthy adults, and ATL cell lines. Primary ATL cells showed a clear 98-kDa band for EZH2 with the absence or presence of faint bands for phosphorylated EZH2 (p-EZH2). Cells from healthy adults hardly showed these bands. ATL cell lines ST1, SO4, and KK1 showed intense bands for both EZH2 and p-EZH2, but LM-Y1 and KOB cells showed intense bands for EZH2 with the absence of a band for p-EZH2. (B) Western blot analysis for histone methylation status was performed. Only primary ATL cells and LM-Y1 and KOB cell lines showed a clear band for H3K27me3, but others hardly showed the band. Bands for H3K27me2, H3K27me1, and histone H3 were observed in almost all samples examined.

Downregulation of miR-101 and miR-128a may be responsible for increased EZH2 expression

So far, more than 700 miRNAs have been identified in humans, and each miRNA regulates multiple target genes. miR-101 and miR-26a have been shown to be negative regulators of *EZH2* expression and are depressed in several types of cancer cells.[34,35] miR-128a is known to be a negative regulator of *BMI1* and has been reported to be involved in glioma cell proliferation.[36] We quantified these miRNAs in primary ATL cells and cells from HTLV-1 carriers to investigate the mechanism of *EZH2* overexpression. ATL cells showed significantly decreased levels of miR-101 and miR-128a compared with the cells from HTLV-1 carriers (Figure 3A and C). Notably, there were significant inverse correlations between *EZH2* expression and miR-101 expression or *EZH2* expression and miR-128a expression (Figure 3D and E), suggesting that decrease of these miRNAs accounts for the overexpression of *EZH2*. Since genomic loss of miR-101 has been reported in prostate cancer,[34] we performed quantitative genomic PCR for miR-101 in two loci, miR-101-1 (chromosome 1p31) and miR-101-2 (chromosome 9p24). Both loci were preserved in all 10 ATL samples examined (*Online Supplementary Figure S4*). The expression of miR-26a did not, in contrast, differ between ATL cells and cells from HTLV-1 carriers (Figure 3B). Unexpectedly, there was no significant correlation between *BMI1* expression and miR-128a expression (Figure 3F).

Adult T-cell leukemia/lymphoma cells are sensitive to DZNep and PS (LBH589)

We first examined the sensitivity of ATL-related cell lines and acute T-lymphoblastic leukemia cell lines to DZNep, an inhibitor of S-adenosylhomocysteine hydrolase, which has recently been shown to decrease the expression of EZH2 and histone methylation.[22,23] DZNep inhibited the proliferation of these cell lines, at concentrations above 0.5 μM (*Online Supplementary Figure S5A*). In contrast, $CD4^+$ T cells from healthy adults as a normal control were resistant to DZNep even at 5 μM. Notably, although DZNep decreased *EZH2* expression in ST1, SO4, and KK1, it did not decrease but rather increased the expression in KOB, results which were confirmed by Western blot (*Online Supplementary Figure S5B and C*). PS (LBH589) is also known to decrease the level of EZH2 in several types of leukemia cells.[24] One hundred nM of PS (LBH589) decreased *EZH2* expression at both transcript and protein levels in ATL cell lines including KOB and LM-Y1, which showed a similar EZH2 expression profile to that of primary ATL cells, namely, high EZH2 expression with low phosphorylated EZH2 and strong H3K27me3 (*Online Supplementary Figure S5D and E*). We next examined whether these agents show a synergistic effect or just an additive effect. As shown in *Online Supplementary Figure S5F* (upper panel), the cell viabilities of LM-Y1 treated with 25 nM PS (LBH589) or 2.5 μM DZNep were 70% and 87%, respectively. A combination of this setting (LBH:DZNep=1:100) markedly decreased the proportion of viable cells (40%) compared with that of cells treated

with either agent alone. Similarly, cell viabilities of KOB treated with 25 nM PS (LBH589), 2.5 μM DZNep, or a combination of these agents were 86%, 93%, and 48%, respectively. By calculating CI according to the method of Chou and Talalay,[29] we found a strong synergistic antiproliferative effect in both cell lines (*Online Supplementary Figure S5F*, lower panel).

Discussion

EZH2 is a critical component of PRC2, which mediates epigenetic gene silencing through trimethylation of H3K27.[37,38] EED and SUZ12 are also required for the exhibition of methyltransferase activity and for the localization of this complex to target genes.[39] In an analysis of genome-wide H3K27 methylation in aggressive prostate cancer tissues, a significant subset of the target genes were also targets in embryonic stem cells, suggesting that the mechanism for gene silencing used to maintain stem cell renewal is converted into oncogenesis.[40] Ectopic expression of EZH2 is capable of providing a proliferative advantage to primary cells, and its gene locus is amplified in primary tumors.[41] Indeed, increased EZH2 expression has been reported in several types of cancer cells, and its clinical significance is extensively studied in prostate cancer.[42] Amounts of both *EZH2* transcript and EZH2 protein were elevated in metastatic prostate cancer; in addition, clinically localized prostate cancers that express higher concentrations of *EZH2* showed a poorer prognosis. An association of increased EZH2 expression with poor prognosis has also been reported in other solid tumors. Currently, however, there are only limited reports describing EZH2 expression in hematologic malignancies.

In the present study, we showed for the first time that EZH2 was over-expressed in ATL cells, and that the increased EZH2 was not phosphorylated and was in its active form. The increased EZH2 seemed to exhibit histone methyltransferase activity *in vivo*, as supported by the results that ATL cells from both peripheral blood and lymph nodes were strongly positive for H3K27me3. Since EZH2 was almost undetectable in cells from healthy adults and HTLV-1 carriers, it is likely that deregulation of PRC2 caused by over-expressed EZH2 is involved in the early steps of ATL oncogenesis. Meanwhile, ATL patients with high EZH2 expression showed shorter survival than patients with low EZH2 expression, indicating that increased EZH2 also plays a role in the process of ATL progression. It has been reported that genes methylated in cancer cells are specifically packaged with nucleosomes containing H3K27.[43] However, there are only a few studies that actually examined H3K27me3 in primary tumor cells or tissues. In one such study, H3K27me3 expression was unexpectedly lower in breast, ovarian, and pancreatic cancers than in corresponding normal tissues, although it has been reported that there are increased levels of H3K27me3 in breast cancer cell lines.[44,45] We do not have an adequate explanation for these conflicts at present, but there may be some differences in the process of oncogenesis between solid tumors and hematologic malignancies.

The mechanism of the overexpression of EZH2 in tumors remains largely unknown. miRNAs regulate gene expression and play important roles in cellular differentiation and embryonic stem cell development. Recently, two miRNAs, miR-101 and miR-26a, were found to repress *EZH2* expression. The expression of miR-101 decreases in parallel with an increase in *EZH2* expression during progression in prostate tumors.[34] In addition to these miRNAs, we examined miR-128a, which has been shown to repress *BMI1* expression in glioblastoma, because overexpression of *BMI-1* is associated with the development of malignant lymphoma.[31,36] ATL cells showed a decreased level of miR-

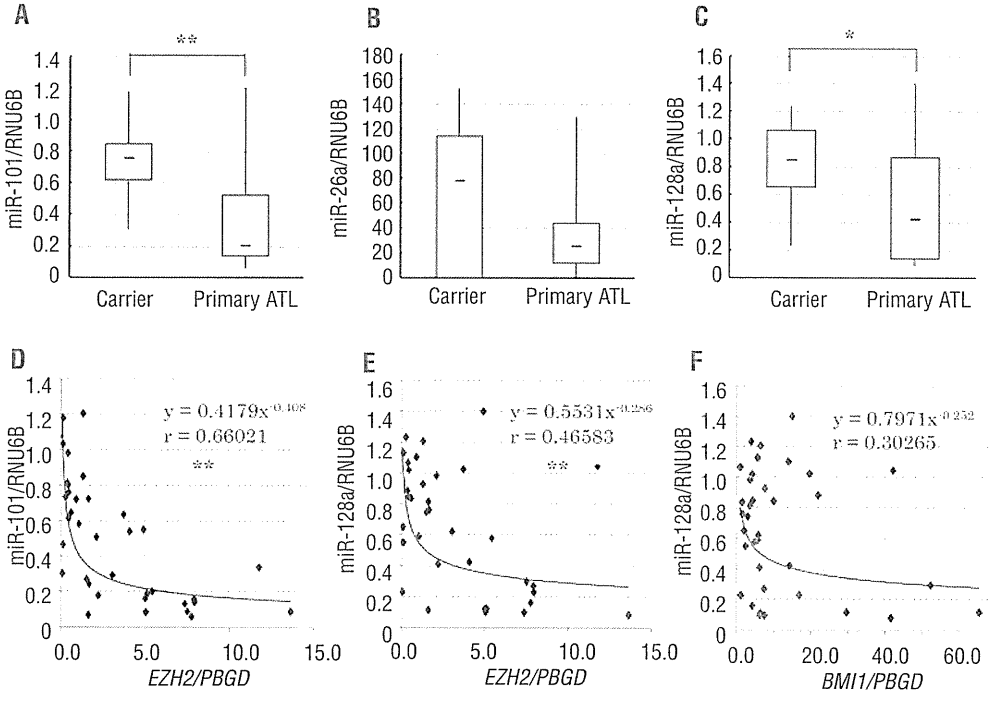

Figure 3. Quantitative real-time RT-PCR for miRNAs. (A-C) Expressions of miR-101 (A), miR-26a (B), and miR-128a (C) were compared between ATL patients and HTLV-1 carriers. Primary ATL cells showed significantly lower levels of miR-101 and miR-128a (Mann-Whitney's U test) compared with the cells from HTLV-1 carriers (A, C). There was no significant difference in miR-26a expression between the two groups (B). (D, E, F) Correlation between miRNA and *EZH2* or *BMI1* expression was examined. There were significant inverse correlations between normalized *EZH2* expression and miR-101 expression (D) or between normalized *EZH2* expression and miR-128a expression (E) (Spearman's correlation coefficient). In contrast, there was no correlation between normalized *BMI1* expression and miR-128a expression (F). $*P<0.05$, $**P<0.01$

101 expression compared with the cells from HTLV-1 carriers, which is not caused by genomic loss of the *miR-101* gene, in contrast to prostate cancer.[34] Moreover, there was a clear inverse correlation between *EZH2* expression and miR-101 expression, suggesting that increased *EZH2* is caused by the decrease in miR-101 expression. Although currently there is no report indicating an association of miR-128a with *EZH2* expression, miR-128a showed exactly the same pattern as miR-101, suggesting that the decrease in miR-128a also participates in *EZH2* overexpression in ATL. By analyzing the 3'-UTR sequence of *EZH2*, it has recently been shown that there are two predicted miR-101 target sites and one predicted miR-26a target site in the 3'-UTR of EZH2.[46] We performed a similar analysis and found that there was also a potential target site for miR-128a near one of the miR-101 target sites (*Online Supplementary Figure S6*). miR-26a was not decreased in ATL cells, and there was no correlation between miR-26a expression and *EZH2* expression or miR-128a expression and *BMI1* expression. The association of miR-26a with *EZH2* was found in normal cell differentiation as a physiological phenomenon but not in tumor cells. The miRNAs used to regulate normal development and differentiation may be different from those used for the development of tumors. Another possible explanation for the mechanism of increased *EZH2* expression in ATL is inactivation of *p14ARF/p15INK4B/p16INK4A* tumor suppressor genes, which frequently occurs in ATL.[14,15,19,20] EZH2 is a molecule downstream of the pRB-E2F pathway, and inactivation of these genes allows E2F to be released from pRB, which results in the upregulation of *EZH2* expression.[41] Several recent reports indicate that EZH2 functions to repress the expression of *p14ARF/p15INK4B/p16INK4A*; therefore, increased EZH2 may be used to further decrease the expression of *p14ARF/p15INK4B/p16INK4A*.[47] Since somatic mutations altering EZH2 (Tyr641) have recently been reported in follicular and diffuse large B-cell lymphomas of germinal-center origin,[48] we performed a similar analysis in 10 primary ATL samples. There were however no such mutations (*Online Supplementary Figure S7*).

ATL is quite resistant to antineoplastic agents and the median survival time of those with the aggressive subtypes is only 13 months, even in a recent multicenter clinical trial.[49] Since high EZH2 expression with H3K27me3 seems to be an essential component for the initiation and promotion of cell proliferation in ATL, we searched for the possibility of therapeutic strategies targeting EZH2. We examined the sensitivity of ATL cells to agents that have been shown to inhibit *EZH2* expression and histone methylation. DZNep is a carbocyclic analog of adenosine synthesized more than 20 years ago as an inhibitor of S-adenosylhomocysteine hydrolase, which has therapeutic potential as an anticancer or antiviral drug.[21] DZNep has recently aroused interest for its unique features; it decreases the expressions of *EZH2*, *SUZ12*, and *EED* with inhibition of H3K27 methylation and induces apoptosis in cancer cells but not in normal cells.[22,23] ATL cell lines were sensitive to DZNep and their cell proliferation was attenuated at one-tenth of the concentration used in these studies. More interestingly, DZNep showed no toxicity to normal $CD4^+$ T cells as a normal control. Acute T-lymphoblastic leukemia cell lines showed similar sensitivities to DZNep, which may indicate that DZNep exerts general toxicity to leukemia and lymphoma cells not necessarily associated with histone modification. Indeed, although DZNep rather increased EZH2 expression in KOB cells, this cell line was equally sensitive as other cell lines to DZNep. HDAC inhibitor PS (LBH589) is an effective agent for cutaneous T-cell lymphoma and induced complete remission in 2 of 9 patients involved in a phase I clinical trial.[50] More interestingly, it has been reported recently that combined use of DZNep and PS (LBH589) yielded more depletion of EZH2 and induced more apoptosis of leukemia cells, but not normal CD34 (+) bone marrow progenitor cells.[51] In the present study, we showed that the combination of DZNep and PS (LBH589) exhibited a synergistic effect in killing ATL cells. Thus, epigenetic therapy by the combined use of these agents that inhibit histone methylation could lead to a breakthrough in the treatment of aggressive ATL.

Authorship and Disclosures

The information provided by the authors about contributions from persons listed as authors and in acknowledgments is available with the full text of this paper at www.haematologica.org.

Financial and other disclosures provided by the authors using the ICMJE (www.icmje.org) Uniform Format for Disclosure of Competing Interests are also available at www.haematologica.org.

References

1. Sparmann A, van Lohuizen M. Polycomb silencers control cell fate, development and cancer. Nat Rev Cancer. 2006;6(11):846-56.
2. Lee TI, Jenner RG, Boyer LA, Guenther MG, Levine SS, Kumar RM, et al. Control of developmental regulators by Polycomb in human embryonic stem cells. Cell. 2006;125(2):301-13.
3. Kamminga LM, Bystrykh LV, de Boer A, Houwer S, Douma J, Weersing E, et al. The Polycomb group gene Ezh2 prevents hematopoietic stem cell exhaustion. Blood. 2006;107(5):2170-9.
4. van Lohuizen M, Tijms M, Voncken JW, Schumacher A, Magnuson T, Wientjens E. Interaction of mouse polycomb-group (Pc-G) proteins Enx1 and Enx2 with Eed: Indication for separate Pc-G complexes. Mol Cell Biol. 1998;18(6):3572-9.
5. Satijn DP, Hamer KM, den Blaauwen J, Otte AP. The Polycomb group protein EED interacts with YY1, and both proteins induce neural tissue in Xenopus embryos. Mol Cell Biol. 2001;21(4):1360-9.
6. van der Vlag J, Otte AP. Transcriptional repression mediated by the human polycomb-group protein EED involves histone deacetylation. Nat Genet. 1999;23(4):474-8.
7. Vire E, Brenner C, Deplus R, Blanchon L, Fraga M, Didelot C, et al. The Polycomb group protein EZH2 directly controls DNA methylation. Nature. 2006;439(7078):871-4.
8. Cao R, Zhang Y. The functions of E(Z)EZH2-mediated methylation of lysine 27 in histoneH3. Curr Opin Genet Dev. 2004;14(2):155-64.
9. Widschwendter M, Fiegl H, Egle D, Mueller-Holzner E, Spizzo G, Marth C, et al. Epigenetic stem cell signature in cancer. Nat Genet. 2007;39(2):157-8.
10. Simon JA, Lange CA. Roles of the EZH2 histone methyltransferase in cancer epigenetics. Mutat Res. 2008;647(1-2):21-9.
11. Uchiyama T, Yodoi J, Sagawa K, Takatsuki K, Uchino H. Adult T-cell leukemia: clinical and hematologic features of 16 cases. Blood. 1977;50(3):481-92.
12. Yoshida M, Seiki M, Yamaguchi K, Takatsuki K. Monoclonal integration of human T-cell leukemia provirus in all primary tumors of adult T-cell leukemia suggests causative role of human T-cell leukemia virus in the disease. Proc Natl Acad Sci USA. 1984;81(8):2534-7.
13. Shimoyama M and members of the Lymphoma Study Group (1984-1987):

Diagnostic criteria and classification of clinical subtypes of adult T-cell leukaemia-lymphoma. A report from the Lymphoma Study Group (1984-1987). Br J Haematol. 1991;79(3):428-37.
14. Hatta Y, Hirama T, Miller CW, Yamada Y, Tomonaga M, Koeffler HP. Homozygous deletions of p15 (MTS2) and p16 (CDKN2/MTS1) genes in adult T-cell leukemia. Blood. 1995;85(10):2699-704.
15. Yamada Y, Hatta Y, Murata K, Sugawara K, Ikeda S, Mine M, et al. Deletions of p15 and/or p16 genes as a poor-prognosis factor in adult T-cell leukemia. J Clin Oncol. 1997;15(5):1778-85.
16. Nagai H, Kinoshita T, Imamura J, Murakami Y, Hayashi K, Mukai K, et al. Genetic alteration of p53 in some patients with adult T-cell leukemia. Jpn J Cancer Res. 1991;82(12):1421-7.
17. Sakashita A, Hattori T, Miller CW, Suzushima H, Asou N, Takatsuki K, et al. Mutations of the p53 gene in adult T-cell leukemia. Blood. 1992;79(2):477-80.
18. Tawara M, Hogerzeil SJ, Yamada Y, Takasaki Y, Soda H, Hasegawa H, et al. Impact of p53 aberration on the progression of adult T-cell leukemia/lymphoma. Cancer Lett. 2006;234(2):249-55.
19. Kohno T, Yamada Y, Tawara M, Takasaki Y, Kamihira S, Tomonaga M, et al. Inactivation of p14ARF as a key event for the progression of adult T-cell leukemia/lymphoma. Leuk Res. 2007;31(12):1625-32.
20. Nosaka K, Maeda M, Tamiya S, Sakai T, Mitsuya H, Matsuoka M. Increasing methylation of the CDKN2A gene is associated with the progression of adult T-cell leukemia. Cancer Res. 2000;60(4):1043-8.
21. Glazer RI, Hartman KD, Knode MC, Richard MM, Chiang PK, Tseng CK, et al. 3-Deazaneplanocin: a new and potent inhibitor of S-adenosylhomocysteine hydrolase and its effects on human promyelocytic leukemia cell line HL-60. Biochem Biophys Res Commun. 1986;135 (2):688-94.
22. Miranda TB, Cortez CC, Yoo CB, Liang G, Abe M, Kelly TK, et al. DZNep is a global histone methylation inhibitor that reactivates developmental genes not silenced by DNA methylation. Mol Cancer Ther. 2009;8(6):1579-88.
23. Tan J, Yang X, Zhuang L, Jiang X, Chen W, Lee PL, et al. Pharmacologic disruption of Polycomb-repressive complex 2-mediated gene repression selectively induces apoptosis in cancer cells. Genes Dev. 2007;21(9): 1050-63.
24. Fiskus W, Pranpat M, Balasis M, Herger B, Rao R, Chinniyan A, et al. Histone deacetylase inhibitors deplete EZH2 and associated Polycomb Repressive Complex 2 proteins with attenuation of HOXA9 and MEIS1 and loss of survival of human acute leukemia cells. Mol Cancer Ther. 2006;5 (12):3096-104.
25. Choi YL, Tsukasaki K, O'Neill MC, Yamada Y, Onimaru Y, Matsumoto K, et al. A genomic analysis of adult T-cell leukemia. Oncogene. 2007;26(8):1245-55.
26. Yamada Y, Ohmoto Y, Hata T, Yamamura M, Murata K, Tsukasaki K, et al. Features of the cytokines secreted by adult T cell leukemia (ATL) cells. Leuk Lymphoma. 1996;21(5-6):443-7.
27. Choi YL, Makishima H, Ohashi J, Yamashita Y, Ohki R, Koinuma K, et al. DNA microarray analysis of natural killer cell-type lymphoproliferative disease of granular lymphocytes with purified CD3(-) CD56(+) fractions. Leukemia. 2004;18(3): 556-65.
28. Hasegawa H, Yamada Y, Komiyama K, Hayashi M, Ishibashi M, Sunazuka T, et al. A novel natural compound, a cycloanthranilylproline derivative (Fuligocandin B), sensitizes leukemia cells to apoptosis induced by tumor necrosis factor related apoptosis-inducing ligand (TRAIL) through 15-deoxy-Delta 12, 14 prostaglandin J2 production. Blood. 2007;110(5):1664-74.
29. Chou TC, Talalay P. Quantitative analysis of dose-effect relationships: the combined effects of multiple drugs or enzyme inhibitors. Adv Enzyme Regul. 1984;22:27-55.
30. Yasunaga J, Taniguchi Y, Nosaka K, Yoshida M, Satou Y, Sakai T, et al. Identification of aberrantly methylated genes in association with adult T-cell leukemia. Cancer Res. 2004;64(17):6002-9.
31. Jacobs JJ, Kieboom K, Marino S, DePinho RA, van Lohuizen M. The oncogene and Polycomb-group gene bmi-1 regulates cell proliferation and senescence through the ink4a locus. Nature. 1999;397(6715):164-8.
32. Scott CL, Gil J, Hernando E, Teruya-Feldstein J, Narita M, Martinez D, et al. Role of the chromobox protein CBX7 in lymphomagenesis. Proc Natl Acad Sci USA. 2007;104(13):5389-94.
33. Cha TL, Zhou BP, Xia W, Wu Y, Yang CC, Chen CT, et al. Akt-mediated phosphorylation of EZH2 suppresses methylation of Lysine 27 in histone H3. Science. 2005;310(5746):306-10.
34. Varambally S, Cao Q, Mani RS, Shankar S, Wang X, Ateeq B, et al. Genomic loss of microRNA-101 leads to overexpression of histone methyltransferase EZH2 in cancer. Science. 2008;322(5908):1695-6.
35. Sander S, Bullinger L, Klapproth K, Fiedler K, Kestler HA, Barth TF, et al. MYC stimulates EZH2 expression by repression of its negative regulator miR-26a. Blood. 2008; 112(10):4202-12.
36. Godlewski J, Nowicki MO, Bronisz A, Williams S, Otsuki A, Nuovo G, et al. Targeting of the Bmi-1 oncogene/stem cell renewal factor by microRNA-128 inhibits glioma proliferation and self-renewal. Cancer Res. 2008;68(22):9125-30.
37. Cao R, Wang L, Wang H, Xia L, Erdjument-Bromage H, Tempst P, et al. Role of histone H3 lysine 27 methylation in Polycomb-group silencing. Science. 2002;298(5595): 1039-43.
38. Czermin B, Melfi R, McCabe D, Seitz V, Imhof A, Pirrotta V. Drosophila enhancer of Zeste/ESC complexes have a histone H3 methyltransferase activity that marks chromosomal Polycomb sites. Cell. 2002;111(2): 185-96.
39. Cao R, Zhang YI. SUZ12 is required for both the histone methyltransferase activity and the silencing function of the EED-EZH2 complex. Mol Cell. 2004;15(1):57-67.
40. Yu J, Yu J, Rhodes DR, Tomlins SA, Cao X, Chen G, et al. A polycomb repression signature in metastatic prostate cancer predicts cancer outcome. Cancer Res. 2007; 67(22):10657-63.
41. Bracken AP, Pasini D, Capra M, Prosperini E, Colli E, Helin K. EZH2 is down stream of the pRB-E2F pathway, essential for proliferation and amplified in cancer. EMBO J. 2003;22(20):5323-35.
42. Varambally S, Dhanasekaran SM, Zhou M, Barrette TR, Kumar-Sinha C, Sanda MG, et al. The polycomb group protein EZH2 is involved in progression of prostate cancer. Nature. 2002;419(6907):624-9.
43. Schlesinger Y, Straussman R, Keshet I, Farkash S, Hecht M, Zimmerman J, et al. Polycomb-mediated methylation of Lys27 of histone H3 pre-marks genes for de novo methylation in cancer. Nat Genet. 2007;39 (2):232-6.
44. Wei Y, Xia W, Zhang Z, Liu J, Wang H, Adsay NV, et al. Loss of trimethylation at lysine 27 of histone H3 is a predictor of poor outcome in breast, ovarian, and pancreatic cancers. Mol Carcinog. 2008;47 (9):701-6.
45. Sun F, Chan E, Wu Z, Yang X, Marquez VE, Yu Q. Combinatorial pharmacologic approaches target EZH2-mediated gene repression in breast cancer cells. Mol Cancer Ther. 2009;8(12):3191-202.
46. Cao P, Deng Z, Wan M, Huang W, Cramer SD, Xu J, et al. MicroRNA-101 negatively regulates Ezh2 and its expression is modulated by androgen receptor and HIF-1alpha/HIF-1beta. Mol Cancer. 2010;9: 108.
47. Bracken AP, Kleine-Kohlbrecher D, Dietrich N, Pasini D, Gargiulo G, Beekman C, et al. The polycomb group proteins bind throughout the INK4A-ARF locus and are disassociated in senescent cells. Genes Dev. 2007;21(5):525-30.
48. Morin RD, Johnson NA, Severson TM, Mungall AJ, An J, Goya R, et al. Somatic mutations altering EZH2 (Tyr641) in follicular and diffuse large B-cell lymphomas of germinal-center origin. Nat Genet. 2010; 42(2):181-5.
49. Yamada Y, Tomonaga M, Fukuda H, Hanada S, Utsunomiya A, Tara M, et al. A new G-CSF-supported combination chemotherapy, LSG15, for adult T-cell leukaemia-lymphoma: Japan Clinical Oncology Group Study 9303. Br J Haematol. 2001;113(2):375-82.
50. Ellis L, Pan Y, Smyth GK, George DJ, McCormack C, Williams-Truax R, et al. Histone deacetylase inhibitor panobinostat induces clinical responses with associated alterations in gene expression profiles in cutaneous T-cell lymphoma. Clin Cancer Res. 2008;14(14):4500-10.
51. Fiskus W, Wang Y, Sreekumar A, Buckley KM, Shi H, Jillella A, et al. Combined epigenetic therapy with the histone methyltransferase EZH2 inhibitor 3-deazaneplanocin A and the histone deacetylase inhibitor panobinostat against human AML cells. Blood. 2009;114(13):2733-43.

Cancer Science
The official journal of the Japanese Cancer Association JCA

Review Article

Oncogenic mutations of *ALK* in neuroblastoma

Seishi Ogawa,[1,2,6] Junko Takita,[3,4] Masashi Sanada[1] and Yasuhide Hayashi[5]

[1]Cancer Genomics Project, The University of Tokyo, Tokyo; [2]Core Research for Evolutional Science and Technology, Exploratory Research for Advanced Technology, Japan Science and Technology Agency, Saitama; [3]Department of Pediatrics, The University of Tokyo, Tokyo; [4]Cell Therapy and Transplantation Medicine, The University of Tokyo, Tokyo; [5]Gunma Children's Medical Center, Gunma, Japan

(Received October 21, 2010/Revised November 26, 2010/Accepted November 28, 2010/Accepted manuscript online December 9, 2010)

Neuroblastoma is one of the most common solid cancers among children. Prognosis of advanced neuroblastoma is still poor despite the recent advances in chemo/radiotherapies. In view of improving the clinical outcome of advanced neuroblastoma, it is important to identify the key molecules responsible for the pathogenesis of neuroblastoma and to develop effective drugs that target these molecules. Anaplastic lymphoma kinase (ALK) is a receptor tyrosine kinase, initially identified through the analysis of a specific translocation associated with a rare subtype of non-Hodgkin's lymphoma. Recently it was demonstrated that *ALK* is frequently mutated in sporadic cases with advanced neuroblastoma. Moreover, germline mutations of *ALK* were shown to be responsible for the majority of hereditary neuroblastoma. ALK mutants found in neuroblastoma show constitutive active kinase activity and oncogenic potentials. Inhibition of ALK in neuroblastoma cell lines carrying amplified or mutated *ALK* alleles results in compromised downstream signaling and cell growth, indicating potential roles of small molecule ALK inhibitors in the therapeutics of neuroblastoma carrying mutated ALK kinases. (*Cancer Sci* 2011; 102: 302–308)

Neuroblastoma is a malignant embryonal neoplasm arising from developing neural crest tissues.[1] It commonly affects younger children, where the median age of diagnosis is 17 months and approximately 90% of the patients are <4 years old. In the United States, the incidence of neuroblastoma is estimated to be one in 7000 births, although the incidence calculated from the mass screening program in Japan was as high as 29.80 cases per 100 000 births, which is significantly higher than the estimation in the prescreening cohort (11.56 cases per 100 000 births).[2] It is the third most common cancer in childhood after leukemia and brain tumors, accounting for 7–11% of all pediatric cancers.[3] The presentation and following clinical courses of neuroblastoma are highly variable, ranging from a solitary localized mass with no apparent clinical symptoms to widely disseminated diseases presenting with severe systemic illness.[1] While some tumors undergo spontaneous regression without therapy, approximately 60–70% of high-risk neuroblastoma patients are resistant to any therapies currently available and succumb to death,[4–6] even though a substantial improvement in 5-year survival rates has been obtained for a subset of advanced tumors through the development of multimodal chemo/radiotherapies during the past several decades.[1] Thus, one of the urgent problems in the current neuroblastoma treatment would be to develop rational and effective therapeutic strategies for the high-risk neuroblastoma cases based on their molecular pathogenesis.

On the other hand, during the past three decades, little advancement has been made in the understanding of neuroblastoma pathogenesis in terms of critical gene targets, except for the identification of frequent *MYCN* amplification.[7] Amplification of the *MYCN* gene is found in approximately 20% of neuroblastoma, especially in advanced diseases, and has been consistently associated with poor prognosis.[8,9] Although *MYCN* amplification is a critical genetic event in neuroblastoma development,[10] it encodes a transcription factor and thus may not be a plausible pharmacological target for therapeutics. Recently, several groups independently discovered activating mutations of the *ALK* gene in the majority of familial neuroblastoma and also in a subset of sporadic neuroblastoma cases.[11–14] Given that the mutated ALK kinases are well-tractable targets for small-molecule kinase inhibitors, the discovery draws attention in the field of neuroblastoma research. In this review, we provide a brief overview of the role of *ALK* mutations in neuroblastoma pathogenesis and their implication in future therapeutics.

Genetic analysis of familial neuroblastoma

One of the first clues to identifying the novel genetic target of neuroblastoma was obtained from a linkage study of neuroblastoma-prone families. It was recognized that approximately 1–2% of newly diagnosed neuroblastoma cases occur within families (familial/hereditary neuroblastoma), indicating the existence of dominantly acting neuroblastoma susceptibility gene(s),[15–19] although previous linkage studies, in an attempt to identify the susceptibility locus, failed to provide a reproducible result due to the insufficient power of the studies.[20–22] Germline mutations of the paired-like homeobox 2B (*PHOX2B*) gene at 4p12 was reported to be responsible for neuroblastoma predisposition, but they were mostly related to a rare form of familial neuroblastoma associated with congenital central hypoventilation syndrome (CCHS) and/or Hirschsprung disease, with rare somatic mutations.[23–26] Recently, researchers at the Pennsylvania University analyzed 20 neuroblastoma pedigrees for linkage using approximately 6000 genetic markers, and mapped a candidate neuroblastoma susceptibility locus to the 2p region between rs18621106 and rs2008535, which contains 104 genes including *MYCN* and *ALK*.[11] Through a resequencing analysis of the *ALK* exons within the pedigrees they identified germline mutations of the *ALK* gene in >90% of the pedigrees that co-segregated with neuroblastoma development within the families, clearly demonstrating that the germline *ALK* mutations are responsible for the susceptibility to the development of hereditary neuroblastoma in the majority of the cases.[11,12] Moreover, the subsequent analysis of *ALK* mutations in sporadic neuroblastoma cases identified a subset of sporadic neuroblastoma cases carrying acquired/germline mutations of *ALK*, which was also reported independently by other groups.[12–14,27]

[6]To whom correspondence should be addressed.
E-mail: sogawa-tky@umin.ac.jp

doi: 10.1111/j.1349-7006.2010.01825.x

Genome-wide copy number scanning of neuroblastoma

These groups conducted genome-wide copy number analyses of neuroblastoma using comparative genomic hybridization (CGH) arrays[12] or single nucleotide polymorphism (SNP) arrays.[11,14,27,28] With thousands to half-a-million genetic probes, both platforms enabled high-throughput detection of subtle genetic changes occurring in tumor genomes.[29,30] Neuroblastoma genomes show characteristic copy number changes that involve large chromosomal segments, including gains of 17q, 1q, 2p and 11p, and losses of 1p, 3p and 11q, which, like other human cancers, collectively comprise a unique genomic profile of neuroblastoma.[11,12,14] High-level amplifications, which usually involve discrete chromosomal regions <1 Mb in length, occurred in approximately 30% of neuroblastoma cases. Approximately 90% of the high-level amplifications in neuroblastoma were centered on the *MYCN* locus at 2p24, whereas other amplicons rarely mutually overlapped, except for the amplifications at 2p23, which exclusively involved the *ALK* locus in common[12,14,28] (Fig. 1).

High-level amplification of the *ALK* gene and aberrantly activated ALK signaling in neuroblastoma was first described by Osajima-Hakomori *et al.*[31] in two neuroblastoma-derived cell lines and a single case of primary neuroblastoma. The genome-wide copy number studies confirmed their finding, in which the frequency of *ALK* amplifications is reported to occur in 3–5% of primary neuroblastoma cases.[11,12,14] Subsequent resequencing studies of *ALK* coding exons disclosed non-synonymous nucleotide substitutions of *ALK* in a subset of sporadic neuroblastoma cases and also of neuroblastoma-derived cell lines with mutation rates of approximately 6–11% and approximately 30%, respectively. Amplified *ALK* alleles, as a rule, did not harbor additional mutations, although in rare cases mutated ALK alleles were amplified.

Genetic abnormalities of the *ALK* gene in human cancers

ALK was initially isolated as a partner of the fusion gene generated by t(2;5)(q23;q35) translocation, which is characteristic of anaplastic large cell lymphoma (ALCL), a rare subtype of non-Hodgkin's lymphoma.[32,33] *ALK* encodes an orphan receptor tyrosine kinase with an apparent molecular mass of 220 kDa. Jelly belly,[34] and pleiotrophin[35] and midkine[36] have been postulated as putative ALK ligands in *Drosophila* and mammalians, respectively, but a dispute about the authentic ligands of ALK still remains. ALK has an extracellular domain that is highly similar to LTK and, together with IGF-1R and c-Ros kinases, belongs to the insulin family of proteins.[37] Expression of ALK is largely restricted to neural tissues and is most abundant in the neonatal brain and, to a lesser extent, in the adult brain.[38–41] In the developing brain, the highest expression was found in the thalamus, mid-brain, olfactory bulb and selected parts of cranial and dorsal ganglia.[38,39] It is of particular note that high frequencies of ALK expression were reported in primary neuroblastoma specimens (22 out of 24 samples) and in other tumor cell lines derived from neuroectdermal tumors including neuroblastoma (13 out of 29 cell lines).[42] These expression patterns of ALK suggest its primary role in normal neural development as well as the pathogenesis of neuroblastoma, although *ALK*-deficient mice seem to show apparently normal develop.[37]

In t(2;5)(q23;q35) translocation, the carbonyl terminal of ALK that contains a kinase domain is fused with nucleophosmin (NPM), generating NPM/ALK fusion protein. *ALK* was also shown to participate in the generation of different fusion genes with a variety of partner genes in ALCL,[43–47] inflammatory fibroblastic tumor,[43,48–52] squamous cell carcinoma of the esophagus[53] and non-small-cell lung cancers (NSCLC).[54,55] In NSCLC, *ALK* was reported to be fused with EML4 to generate EML4–ALK fusion protein as a result of inv(2)(p21p23), which is found in 6% of the NSCLC cases[55] (Fig. 2).

These ALK-containing fusion proteins invariably show constitutive kinase activity and transform NIH3T3 cells and/or confer growth factor independence to 32D and/or Ba/F3 cells.[56–58] When bone marrow cells were retrovirally transduced with *NPM–ALK* and transplanted into mice, they developed B-cell lymphoma within 4 months.[58] The critical role of ALK fusion proteins in neoplastic evolution has been further demonstrated

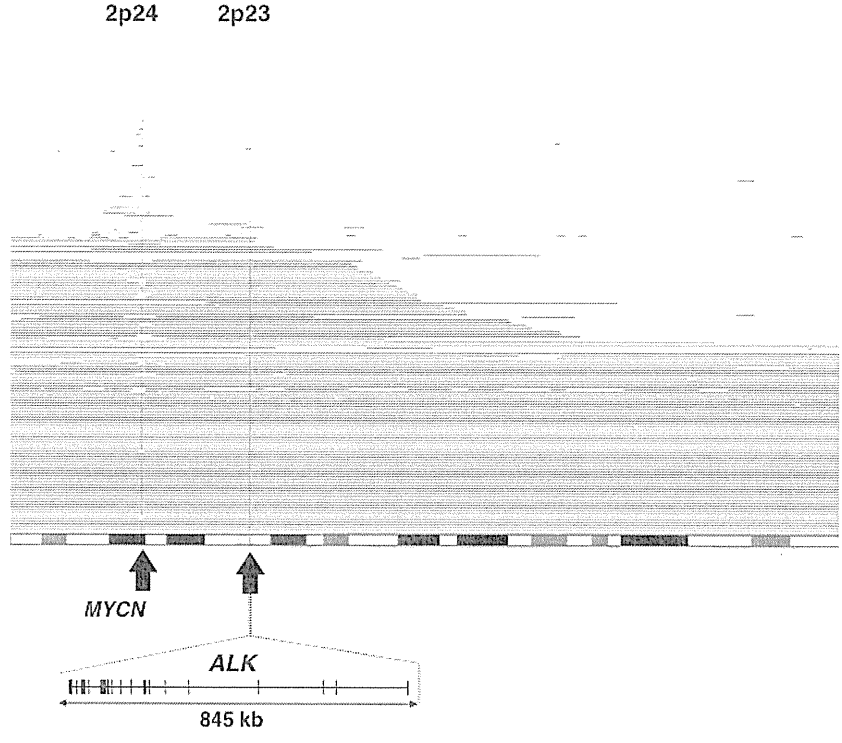

Fig. 1. Copy number gains and high-level amplifications in the short arm of chromosome 2 in neuroblastoma. Each horizontal line indicates a region showing a simple copy number (CN) gain (CN < 5; thick red) and high-level amplification (CN > 5; thin red) in each case. The majority of high-level amplifications involved the *MYCN* locus at 2p24, while the other group of amplicons is found at 2p23, which exclusively contains the *ALK* locus.

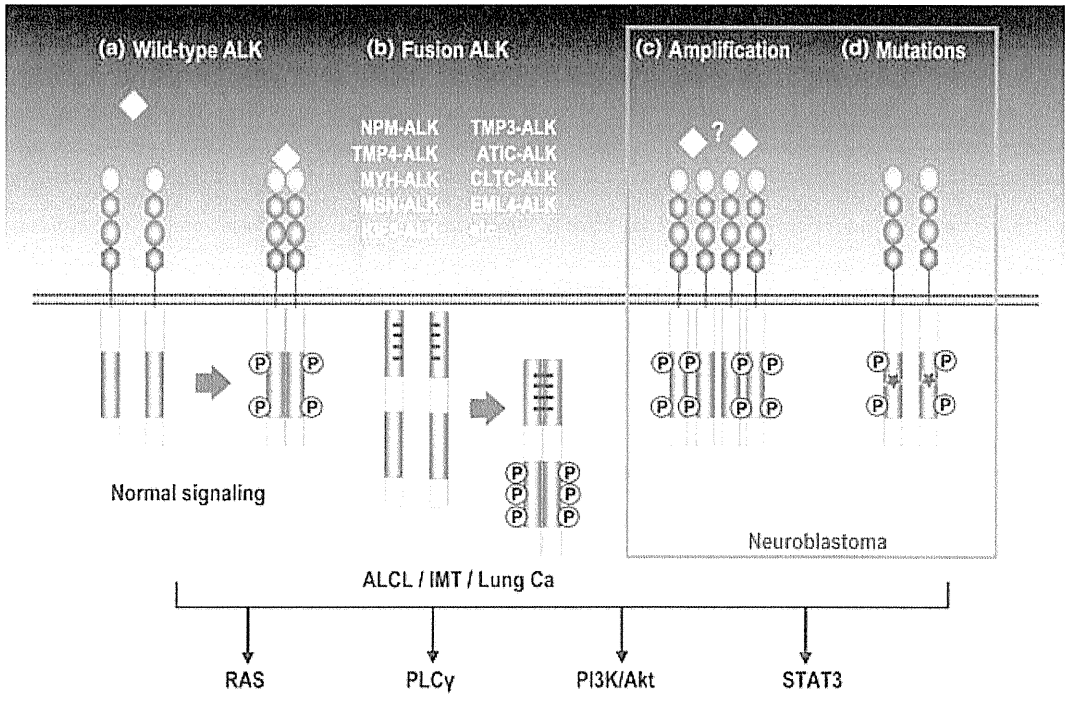

Fig. 2. Aberrant activation of ALK in human cancers. (a) Ligand-dependent physiological activation of wild-type ALK. (b) Fusion ALK kinases found in anaplastic large cell lymphoma (ALCL) and non-small-cell lung cancer (Lung Ca), such as NPM–ALK and EML4–ALK, self-dimerize through their N-terminal domains derived from fusion partners, leading to their transphosphorylation and constitutive activation of the kinase. In a subset of neuroblastoma, aberrant activation of ALK occurs by gene amplification (c) or somatic/germline mutations (d). Activated ALK transmits constitutive signals through downstream pathways, which is thought to be important for tumorigenesis. IMT indicates inflammatory myofibroblastic tumor.

using transgenic mouse models with *ALK* fusion genes; mice carrying *NPM–ALK* or *EML4–ALK* transgenes under *Vav* or *CD4,* or *surfactant protein C* promoter develop aggressive lymphoma or adenocarcinoma of the lung, respectively.[59–61] The aberrant kinase activity of these ALK-fusion proteins is thought to be caused by transphosphorylation upon self-dimerization through their N-terminal domain derived from the fusion partners. Mutations or deletions of the dimerization domain of NPM–ALK and EML4–ALK result in loss of the transforming capacity of the fusion kinases.[55,57] The constitutive active fusion kinases transmit signals through activation of a variety of signal transducers, including PLCγ, PI3K/AKT, STAT3 and RAS.[62–67]

In neuroblastoma, on the other hand, aberrant activation of ALK kinase is caused by gene amplification[31] or mutations.[11–14] Thus, ALK represents a unique type of oncogenic kinase, in that it is deregulated either by gene fusions, or by gene amplification or mutations, depending on the tumor type.

Biological consequences of ALK mutations

Most reported *ALK* mutations occurred within the kinase domain, in which three highly conserved amino acid positions, F1174, F1245 and R1275, were predominantly affected, suggesting their functional importance for the regulation of kinase activity[11–14] (Figs 3,4). The F1174 residue is located at the end of the Cα1 helix and corresponds to equivalent positions mutated in EGFR (V769) and ERBB2 (V769), while the F1245 lies in the catalytic domain and corresponds to the L833 residue of EGFR, a mutation of which is reported to be associated with gefitinib resistance in lung cancer (Fig. 5).[13] The R1275 position lies within the activation loop and is invariably changed to glutamine, and amino acid substitution at this position to a positively charged one would displace the loop to positions that permit autophosphorylation and autoactivation of the kinase (Fig. 5).[68,69] However, the distributions of these mutations were different between sporadic cases and familial cases; R1275 mutations are commonly found in both sporadic and familial cases, while no germline mutations involving the F1174 or F1245 position have been reported.[11–14] Because not all mutant *ALK* carriers develop neuroblastoma (i.e. incomplete penetrance), a germline *ALK* mutation is not fully oncogenic and additional genetic events are thought to be required for neuroblastoma development. *ALK* mutations tend to be associated with advanced diseases and also with *MYCN* amplification in sporadic neuroblastoma cases, although the trend was not clear for germline *ALK* mutations.[11–14]

When expressed in NIH3T3 cells, the predominant kinase domain mutant (F1174L) and a juxtamembrane mutant (K1062M) are shown to have transforming capacity; mutant-transduced cells display increased colony formation in soft agar and tumor generation in nude mice, whereas the mutant kinases show increased autophosphorylation and *in vitro* kinase activity compared with wild-type ALK.[14] In addition, when introduced into an IL-3-dependent cell line, BaF3, the two major kinase domain mutants (F1174L and R1275Q), render the cell line independent of IL-3.[13] Expression of the F1174L mutant in NIH3T3 and Ba/F3 cells leads to constitutive activation of the downstream signaling pathways of the ALK kinase, as demonstrated by increased levels of phosphorylated ERK1/2, STAT3 and AKT.[13,14] These functional and biochemical studies together indicate that these ALK mutants are actually oncogenic and could be responsible for the pathogenesis of neuroblastoma.

doi: 10.1111/j.1349-7006.2010.01825.x

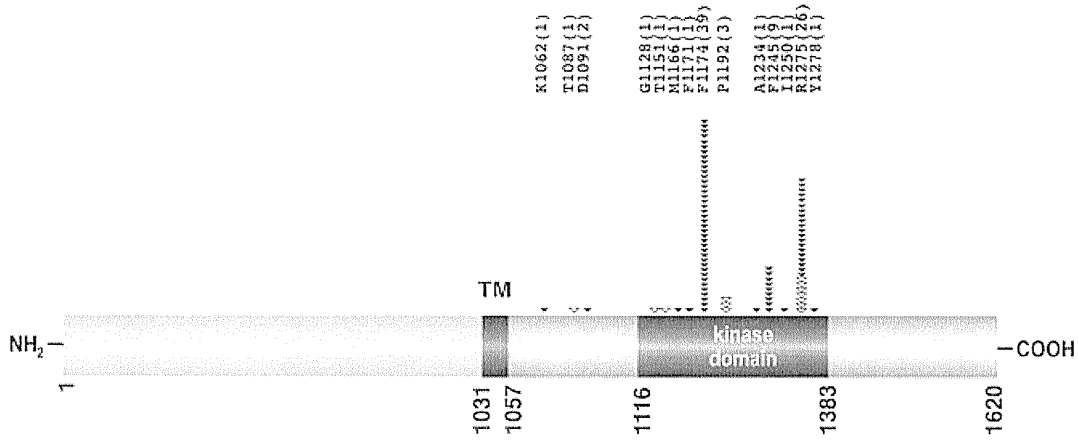

Fig. 3. Frequency and distribution of *ALK* mutations reported in familial and sporadic cases of neuroblastoma.[11–14,27] Locations of somatic and germline mutations of *ALK* in each case or family are depicted by filled and open arrows, respectively. The exact positions and amino acids involved are indicated on the top, where the number of reported mutations is indicated in parenthesis.

```
                    1174
HUMAN ALK     ...ALIISKENHQNIVR..
HUMAN LTK     ...ALIISKERHQNIVR..
HUMAN INSR    ...ASVMKGETCHHVVR..
HUMAN IGF1R   ...ASVMKEENCHHVVR..

                    1245
HUMAN ALK     ...EENHEIHRDIAARN..
HUMAN LTK     ...EENHEIHRDIAARN..
HUMAN INSR    ...NAKKEVHRDLAARN..
HUMAN IGF1R   ...NANKEVHRDLAARN..

                    1275
HUMAN ALK     ...GDFGMARDIYRASY..
HUMAN LTK     ...GDFGMARDIYRASY..
HUMAN INSR    ...GDFGMTRDIYETDY..
HUMAN IGF1R   ...GDFGMTRDIYETDY..
```

Fig. 4. Alignment of amino acids of ALK among different species. Conserved amino-acids among different insulin receptor family kinases are shown by gray boxes and the mutated positions are shown in red.

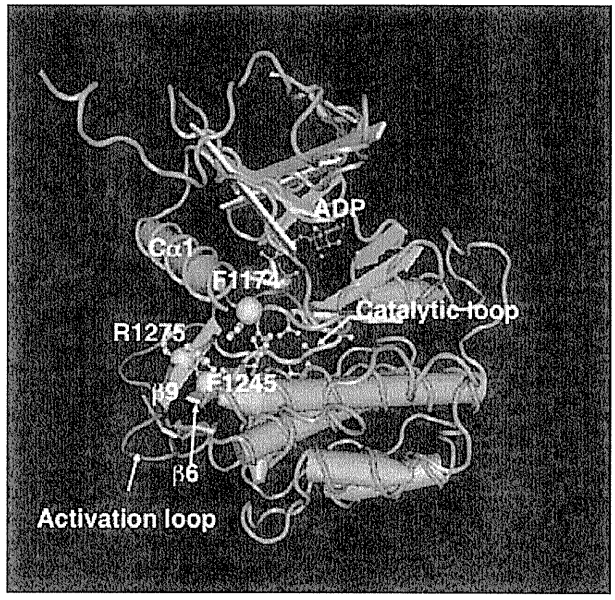

Fig. 5. A 3-D structure of the kinase domain of ALK kinase predicted from that solved for IGF-1R, where the positions of three major mutations are indicated by light blue spheres. Activation and catalytic loops are depicted by red and pink wires.

Effects of ALK inhibition on ALK fusion kinases

The critical role of *ALK* mutations in neuroblastoma development is further supported by the experiments using inhibition of mutant ALK. Tumor suppressive effects of ALK inhibition have been well documented in *NPM–ALK*-positive ALCL and *EML4–ALK*-positive NSCLC. NVP–TAE684 is a highly potent and selective small molecule ALK inhibitor, which blocks the growth of ALCL-derived cell lines with very low IC_{50} values between 2 and 10 nM.[70] NVP–TAE684 treatment of ALCL-derived cell lines induces rapid and sustained inhibition of phosphorylation of NPM–ALK and its downstream signaling, leading to cell cycle arrest and apoptosis.[70] NVP–TAE684 also induces varying degrees of growth suppression in *EML4–ALK*-bearing lung cancer cell lines, including NCI-H3112, NCI-H2228 and DFCI032.[67,71] PF-2341066 was another compound, which was initially identified as an orally available c-Met inhibitor in biochemical enzymatic screens, but was subsequently found to show selective inhibition of ALK.[72,73] It is highly selective for both ALK and c-Met kinases, being almost 20-fold selective for ALK and c-Met compared with 120 other kinases.[73] PF-2341066 inhibited cell growth of NPM–ALK-positive ALCL-derived cell lines, as well as EML4–ALK-positive NSCLC-derived cell lines with decreased downstream signaling pathways, although their IC_{50} values were significantly higher than those of NVP–TAE684.[71,72] Recently, Soda *et al.* generated transgenic mice, in which the *EML4–ALK*-transgene was selectively expressed in the developing lung under the *surfactant protein C* promoter.[61] All mice developed multiple lung adenocarcinomas soon after birth, which were successfully treated with a 2,4-pyrimidinediamine derivative that specifically inhibits ALK kinase.[61] These observations strongly support that aberrant ALK activity of ALK-fusion proteins is central to the development of ALCL and NSCLC.

Effects of ALK inhibition on *ALK*-mutated neuroblastoma cell lines

In neuroblastoma, the predominant mechanism of ALK activation should be some conformational change caused by a point mutation typically involving the kinase domain, which potentially affects the kinetics of ALK inhibitors on the mutated kinase. However, as long as major ALK mutants are concerned, their kinase activity seems to be successfully inhibited by the currently available ALK inhibitors. Ba/F3 cells transduced with the F1174L or R1275Q ALK mutant were effectively killed by NVP–TAE684 or PF-2341066, whereas the cells transduced with a constitutive active FLT3 mutant or wild-type ALK were not.[13] Thus, both compounds specifically inhibit the kinase activity of these ALK mutants, although the inhibition is more efficient for F1174F than for R1275Q. In fact, many, if not all, neuroblastoma cell lines carrying mutated or amplified *ALK* alleles are shown to be sensitive to these ALK inhibitors.[12,13,71] Interestingly, the sensitivity of some neuroblastoma cell lines to small molecule ALK inhibitors was recognized prior to the discovery of *ALK* mutations in neuroblastoma. McDermott *et al.* tested more than 600 cancer cell lines for their sensitivity to NVP-TAE684 and/or PF-2341066 and found that neuroblastoma cell lines, as well as cell lines derived from ALCL and lung cancer, frequently show sensitivity to these inhibitors.[71] The dependence of *ALK*-mutated neuroblastoma to ALK inhibition is further confirmed by ALK knockdown experiments; shRNA-mediated knockdown of ALK in *ALK*-mutated neuroblastoma cell lines results in the suppression of cell growth, indicating that the major effect of ALK inhibitors on *ALK*-mutated neuroblastoma cell lines are mediated by their activity on ALK rather than off-target effects on other kinases.

As mentioned above, the sensitivity of *ALK*-mutated neuroblastoma cell lines to ALK inhibitors seems to substantially differ among cell lines, depending on the type of *ALK* mutations. The F1174L mutant seems to be more sensitive to NVP–TAE684 than the R1275Q mutant.[13] Some *ALK*-mutated cell lines were resistant to ALK inhibition; SMS–KCNR harbors the R1275Q mutation, but was not killed by NVP–TAE684 or shRNA, indicating that this cell line acquired some additional mutations, escaping from its dependence on ALK signaling.

Concluding remarks

Genetic analyses of neuroblastoma have revealed that aberrant activation of ALK kinase in human cancer is not only caused by gene fusions but also by gene amplification or germline/somatic mutations. However, probably the most significant impact of the discovery of *ALK* mutations in neuroblastoma would be the possibility of successful treatment of *ALK*-mutated neuroblastoma with small molecule ALK-inhibitors, which are now under development in several pharmaceutical companies. Because ALK expression is restricted to developing neural tissues and ALK-deficient mice develop normally,[37] mutated ALK is likely to be a plausible therapeutic target. Although the enthusiasm for *ALK*-targeted therapy for advanced neuroblastoma seems to be too early at this moment, an encouraging result was reported from a clinical trial of crizotinib (PF-2341066) for NSCLC carrying the *EML4–ALK* fusion gene. A total of 50 patients were evaluable for response, where 64% of the overall response rate and 90% of the disease control rate were obtained[74] with minimum adverse reactions. Nevertheless, the result in NSCLC is not easily translated into neuroblastoma cases. For example, while some ALK mutants are shown to be inhibited by the available ALK inhibitors *in vitro*, the impact of different mutation types on the action of inhibitors should be further evaluated. The effect of frequent co-existence of *MYCN* amplification with *ALK* mutations on sensitivity to ALK inhibitors is still elusive, although a cell line, KELLY, which carries both the F1174L mutation and *MYCN* amplification, was reported to be sensitive to NVP–TAE684.[13,71] Finally, the role of ALK inhibitors in *ALK*-non-mutated neuroblastoma is another interest. Some neuroblastoma cell lines (NBEBC1 and NB1771) were shown to be sensitive to shRNA-mediated ALK knockdown, even though they were reported to have no mutated *ALK* alleles.[11] Interestingly, ALK is phosphorylated in these cell lines at lower levels. Considering the frequent expression of ALK in neuroblastoma cells, it may be postulated that regardless of its mutation status, ALK play a positive role during the initiation and promotion of neuroblastoma, even though established tumors may or may not depend on the ALK activity. Clearly, much more work is required before the clinical role of ALK inhibitors in the treatment of advanced neuroblastoma is established.

Disclosure Statement

The authors have no conflict of interest.

References

1 Maris JM, Hogarty MD, Bagatell R, Cohn SL. Neuroblastoma. *Lancet* 2007; **369**: 2106–20.
2 Hiyama E, Iehara T, Sugimoto T *et al.* Effectiveness of screening for neuroblastoma at 6 months of age: a retrospective population-based cohort study. *Lancet* 2008; **371**: 1173–80.
3 Brodeur GM. Neuroblastoma: biological insights into a clinical enigma. *Nat Rev Cancer* 2003; **3**: 203–16.
4 Pearson AD, Pinkerton CR, Lewis IJ, Imeson J, Ellershaw C, Machin D. High-dose rapid and standard induction chemotherapy for patients aged over 1 year with stage 4 neuroblastoma: a randomised trial. *Lancet Oncol* 2008; **9**: 247–56.
5 De Bernardi B, Nicolas B, Boni L *et al.* Disseminated neuroblastoma in children older than one year at diagnosis: comparable results with three consecutive high-dose protocols adopted by the Italian Co-Operative Group for Neuroblastoma. *J Clin Oncol* 2003; **21**: 1592–601.
6 Matthay KK, Villablanca JG, Seeger RC *et al.* Treatment of high-risk neuroblastoma with intensive chemotherapy, radiotherapy, autologous bone marrow transplantation, and 13-cis-retinoic acid. Children's Cancer Group. *N Engl J Med* 1999; **341**: 1165–73.
7 Brodeur GM, Seeger RC, Schwab M, Varmus HE, Bishop JM. Amplification of N-myc in untreated human neuroblastomas correlates with advanced disease stage. *Science* 1984; **224**: 1121–4.
8 Seeger RC, Brodeur GM, Sather H *et al.* Association of multiple copies of the N-myc oncogene with rapid progression of neuroblastomas. *N Engl J Med* 1985; **313**: 1111–6.
9 Katzenstein HM, Bowman LC, Brodeur GM *et al.* Prognostic significance of age, MYCN oncogene amplification, tumor cell ploidy, and histology in 110 infants with stage D(S) neuroblastoma: the pediatric oncology group experience – a pediatric oncology group study. *J Clin Oncol* 1998; **16**: 2007–17.
10 Hansford LM, Thomas WD, Keating JM *et al.* Mechanisms of embryonal tumor initiation: distinct roles for MycN expression and MYCN amplification. *Proc Natl Acad Sci U S A* 2004; **101**: 12664–9.
11 Mosse YP, Laudenslager M, Longo L *et al.* Identification of ALK as a major familial neuroblastoma predisposition gene. *Nature* 2008; **455**: 930–5.
12 Janoueix-Lerosey I, Lequin D, Brugieres L *et al.* Somatic and germline activating mutations of the ALK kinase receptor in neuroblastoma. *Nature* 2008; **455**: 967–70.
13 George RE, Sanda T, Hanna M *et al.* Activating mutations in ALK provide a therapeutic target in neuroblastoma. *Nature* 2008; **455**: 975–8.

doi: 10.1111/j.1349-7006.2010.01825.x

14 Chen Y, Takita J, Choi YL *et al.* Oncogenic mutations of ALK kinase in neuroblastoma. *Nature* 2008; **455**: 971–4.
15 Friedman DL, Kadan-Lottick NS, Whitton J *et al.* Increased risk of cancer among siblings of long-term childhood cancer survivors: a report from the childhood cancer survivor study. *Cancer Epidemiol Biomarkers Prev* 2005; **14**: 1922–7.
16 Shojaei-Brosseau T, Chompret A, Abel A *et al.* Genetic epidemiology of neuroblastoma: a study of 426 cases at the Institut Gustave-Roussy in France. *Pediatr Blood Cancer* 2004; **42**: 99–105.
17 Maris JM, Kyemba SM, Rebbeck TR *et al.* Molecular genetic analysis of familial neuroblastoma. *Eur J Cancer* 1997; **33**: 1923–8.
18 Kushner BH, Gilbert F, Helson L. Familial neuroblastoma. Case reports, literature review, and etiologic considerations. *Cancer* 1986; **57**: 1887–93.
19 Knudson AG Jr, Strong LC. Mutation and cancer: neuroblastoma and pheochromocytoma. *Am J Hum Genet* 1972; **24**: 514–32.
20 Longo L, Panza E, Schena F *et al.* Genetic predisposition to familial neuroblastoma: identification of two novel genomic regions at 2p and 12p. *Hum Hered* 2007; **63**: 205–11.
21 Maris JM, Weiss MJ, Mosse Y *et al.* Evidence for a hereditary neuroblastoma predisposition locus at chromosome 16p12-13. *Cancer Res* 2002; **62**: 6651–8.
22 Perri P, Longo L, Cusano R *et al.* Weak linkage at 4p16 to predisposition for human neuroblastoma. *Oncogene* 2002; **21**: 8356–60.
23 Amiel J, Laudier B, Attie-Bitach T *et al.* Polyalanine expansion and frameshift mutations of the paired-like homeobox gene PHOX2B in congenital central hypoventilation syndrome. *Nat Genet* 2003; **33**: 459–61.
24 Mosse YP, Laudenslager M, Khazi D *et al.* Germline PHOX2B mutation in hereditary neuroblastoma. *Am J Hum Genet* 2004; **75**: 727–30.
25 Trochet D, Bourdeaut F, Janoueix-Lerosey I *et al.* Germline mutations of the paired-like homeobox 2B (PHOX2B) gene in neuroblastoma. *Am J Hum Genet* 2004; **74**: 761–4.
26 Raabe EH, Laudenslager M, Winter C *et al.* Prevalence and functional consequence of PHOX2B mutations in neuroblastoma. *Oncogene* 2008; **27**: 469–76.
27 Caren H, Abel F, Kogner P, Martinsson T. High incidence of DNA mutations and gene amplifications of the ALK gene in advanced sporadic neuroblastoma tumours. *Biochem J* 2008; **416**: 153–9.
28 George RE, Attiyeh EF, Li S *et al.* Genome-wide analysis of neuroblastomas using high-density single nucleotide polymorphism arrays. *PLoS ONE* 2007; **2**: e255.
29 Nannya Y, Sanada M, Nakazaki K *et al.* A robust algorithm for copy number detection using high-density oligonucleotide single nucleotide polymorphism genotyping arrays. *Cancer Res* 2005; **65**: 6071–9.
30 Yamamoto G, Nannya Y, Kato M *et al.* Highly sensitive method for genomewide detection of allelic composition in nonpaired, primary tumor specimens by use of affymetrix single-nucleotide-polymorphism genotyping microarrays. *Am J Hum Genet* 2007; **81**: 114–26.
31 Osajima-Hakomori Y, Miyake I, Ohira M, Nakagawara A, Nakagawa A, Sakai R. Biological role of anaplastic lymphoma kinase in neuroblastoma. *Am J Pathol* 2005; **167**: 213–22.
32 Shiota M, Fujimoto J, Takenaga M *et al.* Diagnosis of t(2;5)(p23;q35)-associated Ki-1 lymphoma with immunohistochemistry. *Blood* 1994; **84**: 3648–52.
33 Morris SW, Kirstein MN, Valentine MB *et al.* Fusion of a kinase gene, ALK, to a nucleolar protein gene, NPM, in non-Hodgkin's lymphoma. *Science* 1994; **263**: 1281–4.
34 Lee HH, Norris A, Weiss JB, Frasch M. Jelly belly protein activates the receptor tyrosine kinase Alk to specify visceral muscle pioneers. *Nature* 2003; **425**: 507–12.
35 Stoica GE, Kuo A, Aigner A *et al.* Identification of anaplastic lymphoma kinase as a receptor for the growth factor pleiotrophin. *J Biol Chem* 2001; **276**: 16772–9.
36 Stoica GE, Kuo A, Powers C *et al.* Midkine binds to anaplastic lymphoma kinase (ALK) and acts as a growth factor for different cell types. *J Biol Chem* 2002; **277**: 35990–8.
37 Duyster J, Bai RY, Morris SW. Translocations involving anaplastic lymphoma kinase (ALK). *Oncogene* 2001; **20**: 5623–37.
38 Iwahara T, Fujimoto J, Wen D *et al.* Molecular characterization of ALK, a receptor tyrosine kinase expressed specifically in the nervous system. *Oncogene* 1997; **14**: 439–49.
39 Morris SW, Naeve C, Mathew P *et al.* ALK, the chromosome 2 gene locus altered by the t(2;5) in non-Hodgkin's lymphoma, encodes a novel neural receptor tyrosine kinase that is highly related to leukocyte tyrosine kinase (LTK). *Oncogene* 1997; **14**: 2175–88.
40 Pulford K, Lamant L, Morris SW *et al.* Detection of anaplastic lymphoma kinase (ALK) and nucleolar protein nucleophosmin (NPM)-ALK proteins in normal and neoplastic cells with the monoclonal antibody ALK1. *Blood* 1997; **89**: 1394–404.
41 Shiota M, Fujimoto J, Semba T, Satoh H, Yamamoto T, Mori S. Hyperphosphorylation of a novel 80 kDa protein-tyrosine kinase similar to Ltk in a human Ki-1 lymphoma cell line, AMS3. *Oncogene* 1994; **9**: 1567–74.
42 Lamant L, Pulford K, Bischof D *et al.* Expression of the ALK tyrosine kinase gene in neuroblastoma. *Am J Pathol* 2000; **156**: 1711–21.
43 Cools J, Wlodarska I, Somers R *et al.* Identification of novel fusion partners of ALK, the anaplastic lymphoma kinase, in anaplastic large-cell lymphoma and inflammatory myofibroblastic tumor. *Genes Chromosom Cancer* 2002; **34**: 354–62.
44 Colleoni GW, Bridge JA, Garicochea B, Liu J, Filippa DA, Ladanyi M. ATIC–ALK: a novel variant ALK gene fusion in anaplastic large cell lymphoma resulting from the recurrent cryptic chromosomal inversion, inv(2)(p23q35). *Am J Pathol* 2000; **156**: 781–9.
45 Ma Z, Cools J, Marynen P *et al.* Inv(2)(p23q35) in anaplastic large-cell lymphoma induces constitutive anaplastic lymphoma kinase (ALK) tyrosine kinase activation by fusion to ATIC, an enzyme involved in purine nucleotide biosynthesis. *Blood* 2000; **95**: 2144–9.
46 Trinei M, Lanfrancone L, Campo E *et al.* A new variant anaplastic lymphoma kinase (ALK)-fusion protein (ATIC–ALK) in a case of ALK-positive anaplastic large cell lymphoma. *Cancer Res* 2000; **60**: 793–8.
47 Touriol C, Greenland C, Lamant L *et al.* Further demonstration of the diversity of chromosomal changes involving 2p23 in ALK-positive lymphoma: 2 cases expressing ALK kinase fused to CLTCL (clathrin chain polypeptide-like). *Blood* 2000; **95**: 3204–7.
48 Griffin CA, Hawkins AL, Dvorak C, Henkle C, Ellingham T, Perlman EJ. Recurrent involvement of 2p23 in inflammatory myofibroblastic tumors. *Cancer Res* 1999; **59**: 2776–80.
49 Bridge JA, Kanamori M, Ma Z *et al.* Fusion of the ALK gene to the clathrin heavy chain gene, CLTC, in inflammatory myofibroblastic tumor. *Am J Pathol* 2001; **159**: 411–5.
50 Ma Z, Hill DA, Collins MH *et al.* Fusion of ALK to the Ran-binding protein 2 (RANBP2) gene in inflammatory myofibroblastic tumor. *Genes Chromosom Cancer* 2003; **37**: 98–105.
51 Panagopoulos I, Nilsson T, Domanski HA *et al.* Fusion of the SEC31L1 and ALK genes in an inflammatory myofibroblastic tumor. *Int J Cancer* 2006; **118**: 1181–6.
52 Debelenko LV, Arthur DC, Pack SD, Helman LJ, Schrump DS, Tsokos M. Identification of CARS–ALK fusion in primary and metastatic lesions of an inflammatory myofibroblastic tumor. *Lab Invest* 2003; **83**: 1255–65.
53 Jazii FR, Najafi Z, Malekzadeh R *et al.* Identification of squamous cell carcinoma associated proteins by proteomics and loss of beta tropomyosin expression in esophageal cancer. *World J Gastroenterol* 2006; **12**: 7104–12.
54 Takeuchi K, Choi YL, Togashi Y *et al.* KIF5B–ALK, a novel fusion oncokinase identified by an immunohistochemistry-based diagnostic system for ALK-positive lung cancer. *Clin Cancer Res* 2009; **15**: 3143–9.
55 Soda M, Choi YL, Enomoto M *et al.* Identification of the transforming EML4–ALK fusion gene in non-small-cell lung cancer. *Nature* 2007; **448**: 561–6.
56 Fujimoto J, Shiota M, Iwahara T *et al.* Characterization of the transforming activity of p80, a hyperphosphorylated protein in a Ki-1 lymphoma cell line with chromosomal translocation t(2;5). *Proc Natl Acad Sci U S A* 1996; **93**: 4181–6.
57 Bischof D, Pulford K, Mason DY, Morris SW. Role of the nucleophosmin (NPM) portion of the non-Hodgkin's lymphoma-associated NPM-anaplastic lymphoma kinase fusion protein in oncogenesis. *Mol Cell Biol* 1997; **17**: 2312–25.
58 Kuefer MU, Look AT, Pulford K *et al.* Retrovirus-mediated gene transfer of NPM–ALK causes lymphoid malignancy in mice. *Blood* 1997; **90**: 2901–10.
59 Chiarle R, Gong JZ, Guasparri I *et al.* NPM–ALK transgenic mice spontaneously develop T-cell lymphomas and plasma cell tumors. *Blood* 2003; **101**: 1919–27.
60 Turner SD, Tooze R, Maclennan K, Alexander DR. Vav-promoter regulated oncogenic fusion protein NPM–ALK in transgenic mice causes B-cell lymphomas with hyperactive Jun kinase. *Oncogene* 2003; **22**: 7750–61.
61 Soda M, Takada S, Takeuchi K *et al.* A mouse model for EML4–ALK-positive lung cancer. *Proc Natl Acad Sci U S A* 2008; **105**: 19893–7.
62 Bai RY, Dieter P, Peschel C, Morris SW, Duyster J. Nucleophosmin-anaplastic lymphoma kinase of large-cell anaplastic lymphoma is a constitutively active tyrosine kinase that utilizes phospholipase C-gamma to mediate its mitogenicity. *Mol Cell Biol* 1998; **18**: 6951–61.
63 Bai RY, Ouyang T, Miething C, Morris SW, Peschel C, Duyster J. Nucleophosmin-anaplastic lymphoma kinase associated with anaplastic large-cell lymphoma activates the phosphatidylinositol 3-kinase/Akt antiapoptotic signaling pathway. *Blood* 2000; **96**: 4319–27.
64 Nieborowska-Skorska M, Slupianek A, Xue L *et al.* Role of signal transducer and activator of transcription 5 in nucleophosmin/anaplastic lymphoma kinase-mediated malignant transformation of lymphoid cells. *Cancer Res* 2001; **61**: 6517–23.

65 Slupianek A, Nieborowska-Skorska M, Hoser G *et al.* Role of phosphatidylinositol 3-kinase-Akt pathway in nucleophosmin/anaplastic lymphoma kinase-mediated lymphomagenesis. *Cancer Res* 2001; **61**: 2194–9.
66 Amin HM, McDonnell TJ, Ma Y *et al.* Selective inhibition of STAT3 induces apoptosis and G(1) cell cycle arrest in ALK-positive anaplastic large cell lymphoma. *Oncogene* 2004; **23**: 5426–34.
67 Koivunen JP, Mermel C, Zejnullahu K *et al.* EML4–ALK fusion gene and efficacy of an ALK kinase inhibitor in lung cancer. *Clin Cancer Res* 2008; **14**: 4275–83.
68 Hubbard SR, Mohammadi M, Schlessinger J. Autoregulatory mechanisms in protein-tyrosine kinases. *J Biol Chem* 1998; **273**: 11987–90.
69 Lemmon MA, Schlessinger J. Cell signaling by receptor tyrosine kinases. *Cell* 2010; **141**: 1117.
70 Galkin AV, Melnick JS, Kim S *et al.* Identification of NVP–TAE684, a potent, selective, and efficacious inhibitor of NPM–ALK. *Proc Natl Acad Sci U S A* 2007; **104**: 270–5.
71 McDermott U, Iafrate AJ, Gray NS *et al.* Genomic alterations of anaplastic lymphoma kinase may sensitize tumors to anaplastic lymphoma kinase inhibitors. *Cancer Res* 2008; **68**: 3389–95.
72 Christensen JG, Zou HY, Arango ME *et al.* Cytoreductive antitumor activity of PF-2341066, a novel inhibitor of anaplastic lymphoma kinase and c-Met, in experimental models of anaplastic large-cell lymphoma. *Mol Cancer Ther* 2007; **6**: 3314–22.
73 Zou HY, Li Q, Lee JH *et al.* An orally available small-molecule inhibitor of c-Met, PF-2341066, exhibits cytoreductive antitumor efficacy through antiproliferative and antiangiogenic mechanisms. *Cancer Res* 2007; **67**: 4408–17.
74 Bang Y, Kwak EL, Shaw AT *et al.* Clinical activity of the oral ALK inhibitor PF-02341066 in ALK-positive patients with non-small cell lung cancer (NSCLC). *J Clin Oncol* 2010; **28**(Suppl): abstr3.

doi: 10.1111/j.1349-7006.2010.01825.x